Modelling fine-grained sediment transport in the Mahakam land–sea continuum, Indonesia

Pham Van, Chien; Gourgue, Olivier; Sassi, Maximiliano; Hoitink, Ton; Deleersnijder, Eric; Soares-Frazão, Sandra

DOI
10.1016/j.jher.2015.04.005

Publication date
2016

Published in
Journal of Hydro-Environment Research

Citation (APA)
Pham Van, C., Gourgue, O., Sassi, M., Hoitink, T., Deleersnijder, E., & Soares-Frazão, S. (2016). Modelling fine-grained sediment transport in the Mahakam land–sea continuum, Indonesia. *Journal of Hydro-Environment Research*, *13*, 103-120. https://doi.org/10.1016/j.jher.2015.04.005

Accepted Manuscript

Modelling fine-grained sediment transport in the Mahakam land-sea continuum, Indonesia

Chien Pham Van, Olivier Gourgue, Maximiliano Sassi, A.J.F. Hoitink, Eric Deleersnijder, Sandra Soares-Frazão

PII: S1570-6443(15)00043-X

DOI: 10.1016/j.jher.2015.04.005

Reference: JHER 330

To appear in: *Journal of Hydro-environment Research*

Received Date: 20 August 2014

Revised Date: 9 March 2015

Accepted Date: 5 April 2015

Please cite this article as: Pham Van, C., Gourgue, O., Sassi, M., Hoitink, A.J.F., Deleersnijder, E., Soares-Frazão, S., Modelling fine-grained sediment transport in the Mahakam land-sea continuum, Indonesia, *Journal of Hydro-Environment Research* (2015), doi: 10.1016/j.jher.2015.04.005.

Modelling fine-grained sediment transport in the Mahakam land-sea continuum, Indonesia

Chien Pham Van [1, 2,*], Olivier Gourgue[3, 4], Maximiliano Sassi[5], A.J.F. (Ton) Hoitink [6], Eric Deleersnijder [7, 8], Sandra Soares-Frazão [1]

[1] Institute of Mechanics, Materials and Civil Engineering (IMMC), Université catholique de Louvain, Place du Levant 1, Louvain-la-Neuve, Belgium

[2] Faculty of Hydrology and Water Resources, Water Resources University, Tayson 175, Dongda district, Hanoi, Vietnam.

[3] Department of Hydrology and Hydraulic Engineering (HYDR), Vrije Universiteit Brussel, Pleinlaan 2, Brussels, Belgium.

[4] Flanders Hydraulics Research, Flemish Government, Berchemlei 115, Antwerp, Belgium.

[5] Royal Netherlands Institute for Sea Research, NIOZ, Den Burg, The Netherlands.

[6] Hydrology and Quantitative Water Management Group, Department of Environmental Sciences, Wageningen University, Droevendaalsesteeg 4, Wageningen, The Netherlands.

[7] Institute of Mechanics, Materials and Civil Engineering (IMMC), Université catholique de Louvain, Avenue Georges Lemaître 4, Louvain-la-Neuve, Belgium.

[8] Georges Lemaître Centre for Earth and Climate Research (TECLIM), Earth and Life Institute (ELI), Université catholique de Louvain, Place Louis Pasteur 3, Louvain-la-Neuve, Belgium.

[*] Corresponding author: email:chien.phamvan@uclouvain.be, telephone: +32/10472124, fax: +32/10472179

Abstract

SLIM is an unstructured mesh, finite element model of environmental and geophysical fluid flows, which is being improved to simulate fine-grained sediment transport in riverine and marine water systems. A 2D depth-averaged version of the model is applied to the Mahakam Delta (Borneo, Indonesia), the adjacent ocean, and three lakes in the central part of the Mahakam River catchment. The 2D code is coupled to a 1D section-averaged model for the Mahakam River and four tributaries. The coupled 2D/1D model is mainly aimed at simulating fine-grained sediment transport in the riverine and marine water continuum of the Mahakam River system. Using the observations of suspended sediment concentration (SSC) at five locations in the computational domain, the modelling parameters are first determined in a calibration step, for a given period of time. A validation step is then performed using data related to another period of time. It is concluded that the coupled 2D/1D model reproduces very well the observed suspended sediment distribution within the delta. The spatial distribution of sediment concentration in the delta and its temporal variation are also discussed.

Keywords

Mahakam land-sea continuum, fine-grained sediment, finite element model, coupled 2D/1D model

1. Introduction

Sediments are inherent components of riverine and marine waters, which are transported under the form of fine- or coarser-grained material. The coarser-grained sediment often occurs during episodic and/or anomalous events, e.g. floods or waves associated with strong onshore winds in deltaic or coastal regions (Gastaldo et al., 1995), and usually involves significant bed evolution or morphological changes. On the other hand, considerable attention has been paid to fine-grained sediment transport due to its important role in the fields of coastal engineering, geomorphology, and aquatic ecology (Lou and Ridd, 1997; Turner and Millward, 2002; Hoitink, 2004; Edmonds and Slingerland, 2010; Buschman et al., 2012). High concentration of fine-grained sediment can impact deltaic morphology (Edmonds and Slingerland, 2010), controlling smooth or rough shorelines, flat or complex floodplains of tidal channels as well as navigation and flood mitigation infrastructure. Fine-grained sediment can also result in the degradation of water quality because of the adsorption of organic chemicals and trace metal (Wu et al., 2005; Mercier and Delhez, 2007; Elskens et al., 2014). Therefore, transport and accumulation of fine-grained sediment require to be assessed quantitatively in order to deal with the potential reduction in water quality, the adsorption of toxic substances, and the aquatic food production (van Zwieten et al., 2006; Chaîneau et al., 2010).

Fine-grained sediment particles are moving over the water column and are continuously interacting with the seabed through entrainment or deposition. The movement of sediment particles is caused by a wealth of forces that cannot be represented in detail in most sediment transport model. The submerged weight (i.e. the difference between the gravitational force and Archimedes' buoyancy) tends to pull the particles downward at any time and location, whereas the hydrodynamic force, due to the water flow around every sediment particle, may point upward or downward, depending on the circumstances. The latter force is usually dominated by the drag due to turbulent motion, but this is not the

only phenomenon at work. Clearly, the net sediment flux at the bottom may point downward or upward according to the orientation of the resultant of the forces acting on the sediment particles. The transport of fine-grained sediment inherently indicates complicated processes because of the variation of the flow dynamics and various sediment sources. The latter can consist of (i) sediments originating from terrestrial erosion in the river catchment, riverbed, and river banks, (ii) sediments forming by erosion of coastal areas (van Zwieten et al., 2006), and (iii) sediments re-mobilizing from within the area of interest (Winterwerp, 2013). Moreover, according to Turner and Millward (2002), the transport of fine-grained sediment is particularly complex in deltas and coastal regions, where the prevalence and characteristics of sediment transport are affected by both riverine and marine forcings, e.g. river flow, tide, wind, and waves. Studying fine-grained sediment in a water system under these riverine and marine forcings and various sediment sources is thus one of the major challenges forced by scientists and engineers (Winterwerp, 2013).

Understanding of fine-grained sediment transport processes in a riverine and marine water system is limited by the lack of field measurements and the difficulty to obtain such measurements due to the high spatial and temporal variability of the phenomena at stake. This variability in the system results from various factors, e.g. human activities, availability of sediment sources, changes of land use and soil texture in contributing areas, water discharge and tides. Regarding the modelling of such processes, an integrated approach, which allows for a representation of the transfer of sediment from the river to the coastal ocean and the deep margin, is essential and still is a challenging task. Although existing studies primarily investigate sedimentary processes locally, it is now becoming computationally feasible to adopt an integrated system approach, without excessive simplification of the physical processes resolved by the model. In this context, the present research mainly focuses on simulating in a depth-averaged framework the transport of fine-

grained sediment and its transport in the delta region of the Mahakam land-sea continuum water system.

The Mahakam land-sea continuum is associated with the Mahakam River, which is the second longest river in Kalimantan, Indonesia (Figure 1). Existing studies on fine-grained sediment transport in the Mahakam surface water system are either local, zooming onto particular sites (e.g. Hardy and Wrenn, 2009; Budhiman et al., 2012), or regional, focusing on sedimentary processes in a geological and morphological context (e.g. Gastaldo and Huc, 1992; Gastaldo et al., 1995; Storms et al., 2005). Among the numerical studies performed to investigate the concentration profiles of fine-grained sediment in the modern Mahakam Delta, some have been conducted recently using a three-dimensional finite difference model, ECOMSED, with a structured grid that has a resolution of 200 meters (Hadi et al., 2006; Mandang and Yanagi, 2009). However, such a coarse horizontal grid resolution is unlikely to be suitable to represent both the complex shorelines and the numerous small tidal channels existing in the delta. In addition, these numerical studies validated the modelling parameters over a period of only a few days, and under low flow conditions only, implying that the results obtained in these studies might not be considered as representative of long-term variation of fine-grained sediment in the delta under significant changes of river flow and tides.

A model of fine-grained sediment transport in the Mahakam Delta should be able to cope with a wide range of temporal and spatial scales of several physical processes interacting with each other (de Brye et al., 2011). Therefore, the unstructured mesh, finite element model SLIM (Second-generation Louvain-la-Neuve Ice-ocean Model, www.climate.be/slim) is well suited to the task due to its ability to deal with multi-physics and multi-scale processes in space and time, especially in coastal regions (Deleersnijder and Lermusiaux, 2008). This is because unstructured meshes allow for a more accurate representation of complex coastlines and an increase in spatial resolution in areas of

interest. SLIM solves the shallow-water and advection-diffusion equations including turbulent source terms by using a discontinuous Galerkin finite element scheme for the spatial discretization and second-order diagonally implicit Runge-Kutta time stepping. Although the model was initially developed for simulating flows in coastal areas (e.g. Bernard et al., 2007; Lambrechts et al., 2008b; de Brye et al., 2010; Pham Van et al., under review), the potenial has been widened to simulate sediment transport in estuaries and inland waterways (e.g. Lambrechts et al., 2010; Gourgue et al., 2013).

Regarding the Mahakam Delta and adjacent coastal region of the Mahakam land-sea continuum, whose area is of the order of thousands of square kilometers, using a full-fledged three-dimensional (3D) model for simulating the suspended sediment is likely to exceed the available computer resources. Moreover, as the delta is relatively well-mixed (Storms et al., 2005), a two-dimensional (2D) version of SLIM is believed to be sufficient on the delta and adjacent coastal region, and the one-dimensional (1D) version of SLIM is employed for the rest of the domain (i.e. Mahakam River and tributaries upstream of the delta).

Coupled 2D/1D models have been widely used for practical applications. For example, Wu and Li (1992) applied a coupled 2D/1D quasi-steady model to study sedimentation in the fluctuating backwater region of the Yangtze River (China). Zhang (1999) used a 2D/1D unsteady model to simulate flow and sediment transport in the offshore area near the Yellow River mouth (China). Martini et al. (2004) applied a coupled 2D/1D model for simulating flood flows and suspended sediment transport in the Brenta River (Veneto, Italy). Wu et al. (2005) combined 2D and 1D numerical models to predict the hydrodynamics and sediment transport in the Mersey Estuary (United Kingdom). More recently, de Brye et al. (2010) developed a coupled 2D/1D finite element model for simulating flow dynamics and salinity transport in the Scheldt Estuary and tidal river network, and then Gourgue et al. (2013) developed a sediment module in the same

modelling framework to simulate fine-grained sediment transport. These examples suggest that the transport of fine-grained sediment in the considered system is likely to be dealt with reasonably well by a coupled 2D/1D model.

The main objectives of the present study are (i) to simulate the fine-grained sediment transport within the domain of interest comprising the Mahakam River and tributaries, lakes, the delta as well as the adjacent coastal area of the Mahakam land-sea continuum, (ii) to accurately reproduce the measured sediment concentration at different locations in the system, and (iii) to provide a preliminary investigation of the spatial distribution and temporal variation of sediment concentration in the delta and the tidal river network, under different river flow and tidal conditions. Besides these objectives, it has to be emphasized that the present work is the first attempt to simulate the fine-grained sediment transport in the Mahakam Delta and adjacent coastal region using an unstructured grid, finite element model, which allows for taking into account the very complex geometry and topography of computational domain. Furthermore, to the best of our best knowledge, the current study is also the first one, in which the fine-grained sediment transport from riverine to marine regions is included in one single model so as to capture the interactions between the interconnected regions of the system.

2. Model domain

2.1. Mahakam river-delta-coastal system

The Mahakam Delta is a mixed tidal and fluvial delta, including a large number of actively bifurcating distributaries and tidal channels (Figure 1). The delta is symmetrical and approximately 50 km in radius, as measured from the delta shore to the delta apex. The width of the channels in the deltaic region ranges from 10 m to 3 km. The Mahakam Delta discharges into the Makassar Strait, whose width varies between 200 and 300 km, with a length of about 600 km. Located between the islands of Borneo and Sulawesi, the Makassar Strait is subject to important heat and water transfer from the Pacific to the

Indian Ocean by the Indonesian Throughflow (Susanto et al., 2012). Due to the limited fetch in the narrow strait of the Makassar and low-level wind speed, the mean value of the significant wave height is less than 0.6 m and the wave energy that affects the deltaic processes is very low (Storms et al., 2005). Upstream of the delta is the Mahakam River that meanders over about 900 km. Its catchment area covers about 75000 km^2, with the annual mean river discharge varying from 1000 to 3000 m^3/s (Allen and Chambers, 1998). The middle part of the river is extremely flat. In this area, four large tributaries (Kedang Pahu, Belayan, Kedang Kepala, and Kedang Rantau, see Figure 1) contribute to the river flow and several shallow-water lakes (i.e. Lake Jempang, Lake Melingtang, and Lake Semayang) are connected to the river through a system of small channels. These lakes act as a buffer of the Mahakam River and regulate the water discharge in the lower part of the river in flood situations, by damping flood surges (Storms et al., 2005).

The Mahakam River region is characterized by a tropical rain forest climate with a dry season from May to September and a wet season from October to April. In the river catchment, the mean daily temperature varies from 24 to 29^oC while the relative humidity ranges between 77 and 99% (Hidayat et al., 2012). The mean annual rainfall varies between 4000 and 5000 mm/year in the central highlands and decreases from 2000 to 3000 mm/year near the coast (Roberts and Sydow, 2003). A bimodal rainfall pattern with two peaks of rainfall occurring generally in December and May is reported in the river catchment (Hidayat et al., 2012). Due to the regional climate and the global air circulation, hydrological conditions in the Mahakam River catchment change significantly, especially in ENSO (El Nino-Southern Oscillation) years such as in 1997, leading to significant variations of flow in the river (Hidayat et al., 2012).

2.2. Tidal regime and salinity in the domain of interest

The tide in the Mahakam Delta is dominated by semidiurnal and diurnal regimes, with a predominantly semidiurnal one. The magnitude of the tide decreases from the delta front to

upstream Mahakam River and its value ranges between 1.0 and 3.0 m, depending on the location and the tidal phase (e.g. neap or spring tides). The zone of tidal influence extends up to the lakes region in the middle part of the Mahakam River (Pham Van et al., under review).

The limit of salt intrusion is located around the delta apex (Storms et al., 2005; Pham Van et al., 2012a; Budhiman et al., 2012; Budiyanto and Lestari, 2013). Partial mixing of salinity is reported in the delta, based on the vertical distribution of salinity collected at different locations in the middle region of the delta and in the delta front (Storms et al., 2005; Lukman et al., 2006). According to a recent temperature data collection at 29 locations in the whole delta, the temperature varies from 29.2 to 30.5^{o}C at the surface and from 29.2 to 30.8^{o}C at the bottom (Budiyanto and Lestari, 2013), revealing that there is no large differences of water temperature in the water column and between stations.

Concerning the Mahakam Delta and adjacent coastal region, whose area is of the order of thousands of square kilometers as mentioned previously, using a full-fledged three-dimensional (3D) model for simulating the flow is likely to exceed the available computer resources. Moreover, a very fine grid has to be used to represent many narrow and meandering channels in the delta, thereby increasing the computing time significantly if using 3D models. Thus, a depth-averaged model is designed to be used for simulating the flow dynamics in the delta as well as in the adjacent sea under the present consideration.

2.3. Sediment characteristics in the domain of interest

The deltaic region consists mainly of fine-grained sediment, i.e. particles whose diameter is smaller than 62 μm. Temporal and spatial variations of fine-grained sediment can be influenced by the tides and geometrical factors such as the channel curvature (Dutrieux, 1991; Gastaldo and Huc, 1992; Hardy and Wrenn, 2009; Budhiman et al., 2012). Gastaldo and Huc (1992) investigated the sedimentary characteristics of depositional environments within the delta based on core data, showing that fine-grained sediment is the dominant

component in the vertical sediment profile. Gastaldo et al. (1995) concluded that fine-grained sediment is very common in both the active fluvial distributaries and in the tidal channels of the Mahakam Delta. Recently, Hardy and Wrenn (2009) also reported that fine-grained sediment is dominant in 200 bottom sediment samples that were collected in the Mahakam Delta and the adjacent continental shelf. The suspended load in the delta channels was found to be mainly fine-grained sediment, while the medium to fine sand was considered to be transported as bedload. Budhiman et al. (2012) concluded that the Mahakam coastal waters have a high load of suspended sediment and dissolved matter according to their in situ measurement and remote sensing data.

Recent observations consisting of 106 bed sediment samples that were collected in the period between November 2008 and August 2009 in the Mahakam River reveal that a value of 75% of fine-grained sediment can be found at locations about 120 km upstream from the delta apex (Sassi et al., 2012; 2013). From field measurements, Allen et al. (1979) determined that sediment in the Mahakam River is predominantly fine-grained sediment consisting of silt and clay carried in suspension, with a composition of 70% fine-grained sediment and 30% sand. Those studies show that fine-grained sediments are predominant in the Mahakam River system. That allows models to resort to simple parameterizations of the erosion and deposition processes.

Sassi et al. (2013) reported that three-dimensional effects in the suspended sediment distribution are limited at two deltaic bifurcations located around the delta apex, and restricted to an upstream region of the Mahakam River. They also showed that the Rouse number, which is defined as the ratio of sediment settling velocity to the shear velocity of the flow and von Karman constant (≈0.41), can be estimated based on the Rouse distribution of suspended sediment concentration (SSC). Using the measured profiles of flow velocity and suspended sediment concentration, Sassi et al. (2013) reported that the Rouse number is typically equal to 0.3 at these two deltaic bifurcations. These

considerations suggest that a depth-averaged model can be used to simulate the suspended sediment dynamics in the delta.

3. Hydrodynamic module

3.1. Computational grid

The computational domain is divided into one-dimensional (1D) and two-dimensional (2D) sub-domains. The 2D sub-domain covers the Makassar Strait, the various channels of the delta, and the three largest lakes in the middle part of the Mahakam River. The Mahakam River and four tributaries are represented as 1D sub-domains (Figure 2). The 2D sub-domain uses an unstructured grid (made of a series of triangles) whose resolution varies greatly in space. It features a very detailed representation of the delta. The spatial resolution is such that there are at least two triangles (or elements) over the channel width of each tidal branch or creek in the delta. The element size varies over a wide range, from 5 m in the narrowest branches of the delta to around 10 km in the deepest part of the Makassar Strait. The river network within the 1D sub-domain has a resolution of about 100 m between cross-sections. The unstructured grid shown in Figure 2, which comprises 60819 triangular elements and 3700 1D line segments, is generated using the open-source mesh generation software GMSH (www.geuz.org/gmsh), which is described in detail in Lambrechts et al. (2008a) and Geuzaine and Remacle (2009).

An unstructured grid comprising only the main deltaic channels was used by de Brye et al. (2011) who quantified the division of water discharge through the main channels of the Mahakam Delta. Then, Sassi et al. (2011) used the same unstructured grid for numerical simulations, aimed at studying the tidal impact on the division of water discharge at the bifurcations in the delta. In comparison with the computational grid of the Mahakam Delta reported in the abovementioned previous studies, the current computational grid presents an improvement in the representation of the delta, i.e. most meandering and tidal branches

and the creeks in the delta are now taken into account together with the main deltaic channels.

The use of the unstructured grid allows to accuratedly represent very complex shorelines. The refinement of the grid resolution takes into account (i) the spatial variation of bathymetry and (ii) the distance to the delta apex in order to cluster grid nodes in regions where small scale processes are likely to take place. The use of a model with such refinement is an important achievement, because a wide range of temporal and spatial scales of several physical processes interacting with each other in narrow and meandering tidal branches can be represented in the simulations.

3.2. Governing equations

In the 2D computational domain, the free surface water elevation η, positive upward, and the depth-averaged horizontal velocity vector, $\mathbf{u}=(u, v)$, in the hydrodynamic module are computed by solving the depth-averaged shallow-water equations, i.e.

$$\frac{\partial \eta}{\partial t}+\nabla\cdot\left(H\mathbf{u}\right)=0 \tag{1}$$

$$\frac{\partial \mathbf{u}}{\partial t}+\mathbf{u}\cdot\left(\nabla\mathbf{u}\right)+f\mathbf{k}\times\mathbf{u}+g\nabla\eta=\frac{1}{H}\nabla\cdot\left[H\nu\left(\nabla\mathbf{u}\right)\right]-\frac{\boldsymbol{\tau}_{\mathbf{b}}}{\rho H} \tag{2}$$

where t is the time and ∇ is the horizontal del operator; $H=\eta+h$ is the water depth, with h being the water depth below the reference level; $f=2\omega\sin\phi$ is the Coriolis parameter, where ω is the Earth's angular velocity and ϕ is the latitude; $\mathbf{k}$ is the unit upward vector; g, ρ and ν are the gravitational acceleration, the water density (assumed to be constant under the Boussinesq approximation) and the horizontal eddy viscosity, respectively; $\boldsymbol{\tau}_{\mathbf{b}}$ is the bottom shear stress vector which is parameterized using the Chezy-Manning-Strickler formulation,

$$\boldsymbol{\tau}_{\mathbf{b}}=\rho\frac{gn^2\left\|\mathbf{u}\right\|}{H^{1/3}}\mathbf{u} \tag{3}$$

with n being the Manning friction coefficient. The Manning coefficient is calibrated to reproduce the flow dynamics as well as possible.

The horizontal eddy viscosity is evaluated using the Smagorinsky eddy parameterization method (Smagorinsky, 1963).

$$\nu = (0.1\Delta)^2 \sqrt{2\left(\frac{\partial u}{\partial x}\right)^2 + \left(\frac{\partial u}{\partial y} + \frac{\partial v}{\partial x}\right)^2 + 2\left(\frac{\partial v}{\partial y}\right)^2} \quad (4)$$

where Δ is the local characteristic length scale of the element, i.e. the longest edge of a triangle in the 2D unstructured mesh. Using the Smagorinsky eddy parameterization, the horizontal eddy viscosity is a function of the gradient of the velocity components and of the local mesh size. This improves the representation of local subgrid scale phenomena.

Although the hydrodynamics in the delta region can be affected to some extent by the wind, the influence of the wind is not taken into account in this study, because large parts of the open water in the domain of interest are sheltered from wind action by vegetation. In the lakes, the effects of wind are not considered too because there are no suitable data for this region.

Several nodes and elements in the computational domain, especially close to the deltaic area, can undergo wetting and drying processes, depending on the water elevation and tidal conditions at each time step. Therefore, a special treatment of these transition elements or moving boundaries is required. In this paper, we use the wetting and drying algorithm designed by Kärnä et al. (2011). This means that the actual bathymetry (i.e. the water depth h below the reference level) is modified according to a smooth function $f(H)$ as $h+f(H)$, to ensure a positive water thickness at any time. The smooth function has to satisfy the following properties. Firstly, the modified water depth (i.e. $\eta+h+f(H)$) is positive at any time and position. Secondly, the difference between the real and modified water depths is negligible when the water depth is significantly positive. Thirdly, the smooth function is continuously differentiable to ensure convergence of Newton iterations when using an implicit time stepping. The following function, which satisfies the properties described above, is used:

$$f(H)=\frac{1}{2}\left(\sqrt{H^2+\theta^2}-H\right) \quad (5)$$

where θ is a free parameter controlling the smoothness of the transition between dry and wet situations. In our calculations, a value θ=0.5 m is selected for modifying the bathymetry, in order to maintain the positive water depth.

The wetting and drying algorithm designed by Kärnä et al. (2011) satisfies continuity and momentum conservation, and the full mass conservation in a way that is compatible with the tracer equation. This method can also be implemented in an implicit framework, which enables the CPU time to be significantly reduced by using a large time step, as shown in next section. Further information on the wetting and drying algorithm can be found in Kärnä et al. (2011).

In the 1D sub-domain comprising the Mahakam River and tributaries, the continuity and momentum equations are integrated over the river cross-section, yielding the following form:

$$\frac{\partial A}{\partial t}+\frac{\partial (Au)}{\partial x}=0 \quad (6)$$

$$\frac{\partial u}{\partial t}+u\frac{\partial u}{\partial x}+g\frac{\partial \eta}{\partial x}=\frac{1}{A}\frac{\partial}{\partial x}\left(\nu A\frac{\partial u}{\partial x}\right)-\frac{\tau_b}{\rho H} \quad (7)$$

where A is the cross-sectional area, $H=A/b$ is here the effective flow depth and b is the river width. The eddy viscosity is parameterized using the zero-equation turbulent model, under the form:

$$\nu=\lambda u_* H \quad (8)$$

where λ is a non-dimensional eddy viscosity coefficient that is given the value of 0.16 in the present study (Darby and Thorne, 1996; Pham Van et al., under review), and u_* is the friction shear velocity, which is calculated as $u_*^2=c_f u^2$, with c_f being a coefficient obtained from Manning's formula ($c_f=gn^2H^{-1/3}$). The bottom shear stress τ_b in the 1D model is computed as:

$$\tau_b = \rho \frac{g n^2 |u|}{H^{1/3}} u. \quad (9)$$

It is worth noting that bed evolution can occur due to the erosion and deposition of sediments, which can in turn influence the flow. However, as reported in our previous study (Pham Van et al., 2012b), the effects of the bed evolution caused by sediment erosion and deposition on the flow are not significant in this case. For example, when including and excluding the bed evolution resulting from sediment erosion and deposition in the model, the difference in the norm of the velocity at different locations (e.g. Muara Karman, Samarinda, Delta Apex, Delta North, and Delta South in Figure 2) is less than 0.006 m/s while the difference in water depth is less than 0.005 m. Therefore, the morphological evolution is not considered in the present study.

3.3. Finite element implementation

The governing equations for flow dynamics are solved in the framework of the finite element model SLIM by using an implicit discontinuous Galerkin finite element method that is described in detail in Comblen et al. (2010), de Brye et al. (2010), Kärnä et al. (2011), and the related references therein. Thus, only general information about the finite element implementation is provided here to avoid a repeated description of the model and its capabilities. The computational domain is discretized into a series of triangles or elements as shown in Figure 2. The governing equations are multipled by test functions and then integrated by parts over each element, resulting in element-wise surface and contour integral terms for the spatial operators. The surface term is solved using the DG-FEM with linear shape function, while a Roe solver is used for computing the fluxes at the interfaces between two adjacent elements to represent the water-wave dynamics in contour terms properly (Comblen et al., 2010). At the interface between the one and two dimensional models, local conservation is warranted by compatible 1D and 2D numerical fluxes (de Brye et al., 2010). At the interface of a bifurcation/confluence point in the 1D model, numerical fluxes are computed by using the continuity of mass and momentum and

by imposing the characteristic variables described from eq. (6) and (7) (Pham Van et al., under review). A second-order diagonally implicit Runge-Kutta method is used for the temporal derivative operator (Kärnä et al., 2011). The time increment Δt=10 minutes is chosen for all calculations in this study.

3.4. Bathymetry

The bathymetry data obtained in the year 2008 and 2009 are employed to represent the delta, the lakes, and the river. The depth in all channels varies greatly, generally in a range between 5 to 45 m. The depth remains typically about 5 m in the three lakes located in the middle area of the Mahakam River. In the Mahakam River and its four largest tributaries, the observed bathymetry data are used to interpolate the channel cross-section wetted area at different water elevations. Further information on the bathymetry data obtained from fieldwork campaigns and the interpolation procedures can be found in Sassi et al. (2011). The bathymetry data from the global GEBCO (www.gebco.net) database are used in the Makassar Strait and for the adjacent continental shelf.

3.5. Boundary and initial conditions

The tides from the global ocean tidal model TPXO7.1 (Egbert et al., 1994) are imposed at downstream boundaries through elevation and velocity harmonics while the daily time-series of water discharge are provided at the upstream boundary. The open sea downstream boundaries are located far away from the delta, i.e. at the entrance and exit of the Makassar Strait (Figure 2a). As upstream boundary condition, the measured water discharge (Hidayat et al., 2011) is imposed at the city of Melak (for the Mahakam River), where the tidal influence on the flow is negligible, and the other upstream boundaries in four tributaries (Figure 2b). As detailed below, different flow periods are chosen for calibration simulations, aimed at determining the modelling parameters in the suspended sediment transport module, and for validation of those parameters.

The initial flow velocity in the computational domain is set equal to zero and an arbitrary value of 0.5 m is used for the initial water elevation, except in the three lakes where a calculated value of water elevation is imposed. A spin up period of one neap-spring tidal cycle (about 15 days) is applied before starting the effective simulations during the period of interest, so as to make sure that all transients effects associated with the initialization are dissipated. This spin up period is largely sufficient, as it was observed that regime conditions are already reached after a few days.

3.6. Validation

The main parameter to be calibrated in the hydrodynamic module is the Manning coefficient. This parameter is adjusted by comparing model results with continuous observations of water elevation at six stations (*blue dots* in Figure 2), of the velocity at Samarinda station, and of the water discharge at five stations (*red squares* in Figure 2) (Pham Van et al., under review). The optimal values of the bottom friction obtained from the calibration and validation steps consist of (i) a constant value of 0.023 ($s/m^{1/3}$) for the Makassar Strait, (ii) a linearly increasing value in the delta region, from 0.023 ($s/m^{1/3}$) in the coastal region to 0.0275 ($s/m^{1/3}$) in the region from the delta front to the delta apex, (iii) a constant value of 0.0275 ($s/m^{1/3}$) in the Mahakam River and its four tributaries, and (iv) a larger value of 0.0305 ($s/m^{1/3}$) in the lakes.

Selected results of flow dynamics, obtained by using the abovementioned optimal values of the Manning coefficient, are shown in Figure 3 illustrating comparisons of the water elevation at Delta North (Figure 3b) and Delta South (Figure 3c) stations and the velocity at Samarinda station (Figure 3d). As shown in Figure 3b-c, the model simulates the observed water elevation at Delta North and Delta South very well. The root mean square (RMS) error of water elevation is less than 10 cm and this error is only about 4% of the observed magnitude of water elevation at the station. In addition, it is obvious that the model also adequately reproduces the observed velocity at Samarinda (Figure 3d) in the

period from 11-19-2008 to 12-02-2008. The RMS error of velocity is 0.06 m/s, about 8% of the observed magnitude of measured velocity. A slight discrepancy of water elevation and an overestimation of velocity at high tidal situations can be explained by the uncertainty on the prescribed water discharge at the upstream tributaries and by our model ignoring secondary flows.

4. Suspended sediment module

4.1 Governing equations

The two-dimentional depth-averaged equation for SSC takes the form below.

$$\frac{\partial(HC_{ss})}{\partial t}+\nabla\cdot(HuC_{ss})=\nabla\cdot(H\kappa\nabla C_{ss})+E-D \tag{10}$$

where C_{ss} is the depth-averaged SSC (kg/m^3); κ is the diffusivity coefficient; and E and D are the erosion and deposition rates, respectively. The difference between erosion and deposition rates or net sediment exchange is the source term in the governing equation (10), allowing for a correct representation of the SSC.

In the 1D sub-domain, the SSC is determined by solving the cross-section averaged advection-diffusion equation

$$\frac{\partial(AC_{ss})}{\partial t}+\frac{\partial(AuC_{ss})}{\partial x}=\frac{\partial}{\partial x}\left(A\kappa\frac{\partial C_{ss}}{\partial x}\right)+b(E-D). \tag{11}$$

The diffusivity coefficient κ is parameterized using the Okubo formulation (Okubo, 1971)

$$\kappa=c_k\Delta^{1.15}, \tag{12}$$

where c_k is an appropriate coefficient. A constant value c_k=0.018, which is calibrated from the best fit to the available salinity data in the model domain (see Appendix A), is applied to determine the diffusivity coefficient. Note that the characteristic local length scale of the grid Δ is the length of a segment (i.e. the distance between two river cross-sections) in the 1D mesh.

4.2 Erosion rate

Suspended sediment transport is generally described as a purely physical process, resulting from the response of sediment beds to hydrodynamic forces in coastal regions (Le Hir et al., 2007). Sediment can be eroded from the bed and resuspended into the water column under certain flow conditions. In this study, an infinite sediment supply from the bed is assumed so that only flow conditions control the erosion processes. This approximation is adopted because of the rather limited bed sediment data in the computational domain. Using this approximation, regime conditions are reached after a rather short spin-up period.

The erosion rate E can be determined using different empirical formulas from the literature, adapted to the considered environment. For example, in fine-grained sediment environments, the empirical formula originally proposed by Partheniades (1965) is commonly used for evaluating the erosion rate (e.g. Lang et al. 1989, Sanford and Maa, 2001; Wu et al., 2005; Mercier and Delhez, 2007; Gong and Shen, 2010; Gourgue et al., 2013; Winterwerp, 2013). Thus, in the present consideration, in which fine-grained sediment is mainly focused on, the erosion rate of fine-grained sediment eroded from the bed is also parameterized with the empirical formula introduced by Partheniades (1965) as in many other studies mentioned above.

$$E = \begin{cases} M\left(\dfrac{\tau_b}{\tau_c} - 1\right)^m & if \quad \tau_b > \tau_c \\ 0 & if \quad \tau_b \le \tau_c \end{cases} \tag{13}$$

where τ_b is the norm of the bottom shear stress vector $\boldsymbol{\tau_b}$ in the 2D model or the norm of the bottom shear stress τ_b in the 1D model, τ_c is the critical shear stress for sediment erosion, M is the erosion rate parameter, and m is the relevant exponent. The exponent m is set equal to unity, as in the original formulation of Partheniades (1965). Both τ_c and M are related to the physical and chemical characteristics of sediments, e.g. dry density, mineral composition, organic material, and temperature. Typical value of τ_c varies between 0.02

and 1.0 N/m^2 (Neumeier et al., 2006; Le Hir et al., 2007). A value τ_c=0.1 N/m^2, which is used by Mandang and Yanagi (2009) for the Mahakam Delta, is adopted herein. This value is also commonly used as a threshold value in studies of erosion of fine-grained sediment in rivers and lakes (Kirk Ziegler and Nisbet, 1994; 1995). Typical values of *M* range from 0.00004 to 0.00012 kg/m^{2}s (Wu et al., 2005; Mercier and Delhez, 2007). The value of this parameter is optimized using the observed field data of SSC at five locations (Table 1).

4.3 Deposition rate

The deposition rate of fine-grained sediment is calculated according to the formulation by Einstein and Krone (1962), as in many other studies (e.g. Wu et al., 2005; Mercier and Delhez, 2007; Mandang and Yanagi, 2009; Gong and Shen, 2010; Winterwerp, 2013):

$$D = P_1 w_s C_{ss} \tag{14}$$

where w_s is the setting velocity and P_1 is the probability of deposition. The approach proposed by Ariathuri and Krone (1976) is applied to compute the probability of deposition. This means that the probability of deposition is given by

$$P_1 = \begin{cases} 1 - \dfrac{\tau_b}{\tau_d} & if \quad \tau_b \le \tau_d \\ 0 & if \quad \tau_b > \tau_d \end{cases} \tag{15}$$

where τ_d is the critical shear stress for deposition of sediment. The value of the critical shear stress for the deposition of sediment depends on sediment type and concentration (Mehta and Partheniades, 1975) and its value ranges between 0.06 and 1.1 N/m^2. Regarding the Mahakam water surface system, field investigation of the critical shear stress for deposition of sediments is rather limited and in order to make the calibration of parameters as simple as possible, the value of τ_d is set equal to the value of τ_c in this study.

The settling velocity is parameterized as a function of sediment concentration, under the form (Van Leussen, 1999; Wu, 2007).

$$w_s = k_1 C_{ss}^{\beta} \tag{16}$$

where k_1 is an empirical parameter and β is the appropriate exponent. The value of k_1 can vary in a range between 0.01 and 0.1 (Gourgue et al., 2013). The exponent β can vary over a wide range, depending on the type of particles in suspension and on the flow. Burban et al. (1990) mentioned that an approximate value β=-0.024 and β=0.28 could be applied for freshwater and seawater environments, respectively, while its value varies between 0.5 and 3.5 according to Van Leussen (1999), and between 1 and 2 according to Wu (2007). In this study, the constant k_1 and exponent β are treated as calibration parameters. This means there are three parameters (i.e. M, β, and k_1) that need to be calibrated in the suspended sediment module.

4.4 Finite element implementation

As for the hydrodynamic module, the governing equations, i.e. (10) and (11), for suspended sediment are solved in the framework of the finite element model SLIM by using an implicit discontinuous Galerkin finite element method. The governing equations are discretized on the unstructured mesh shown in Figure 2, using the same discretization as the shallow-water equations. Then, local/global conservation and consistency are warranted for the tracers (White et al., 2008). Stability is ensured by computing the fluxes at the interface between two triangles using an upwind scheme. The same time-stepping scheme is used as in the hydrodynamic module, i.e. second-order diagonally implicit Runge-Kutta with a time step of 10 minutes. At the interface between 1D and 2D sub-domains, local conservation is warranted by compatible 1D and 2D numerical fluxes (de Brye et al., 2010).

4.5 Boundary and initial conditions

The SSC is set equal to zero at the open sea boundaries while a constant value of SSC in the range between 0.03 and 0.25 (kg/m^3) is imposed for the upstream boundary in the Mahakam River and the four tributaries. Because no other data are available, the value at each upstream tributary is simply interpolated from the catchment-area ratio and an

averaged SSC value in the river system. The latter is preliminarily estimated from the averaged sediment discharge (8×10^6 m^3/year) and annual river discharge (between 1000 and 3000 m^3/s) which are reported in (Allen and Chambers (1998). In the reality, because sediments are not always available, a long period of small SSC can have an influence on the SSC in the delta. Nevertheless, this does not occur frequently and this drawback of the model has a negligible influence on the results.

The initial condition of SSC in the computational domain is set to 0.005 kg/m^3 except in the Makassar Strait, where a nil value is employed. A spin up period of one neap-spring tidal cycle (about 15 days) is applied before the period of interest. The regime condition for SSC is obtained a few days after the hydrodynamic regime conditions.

5. Calibration and validation of the suspended sediment module

5.1. Available data

The suspended sediment data cover different periods, under varying tidal conditions (i.e. neap and spring tides) in the survey period between November 2008 and August 2009. Surveys took place (Figure 2) over river sections in the city of Samarinda, at two locations downstream of the delta apex bifurcation (denoted by DAN and DAS), and at two locations downstream of the first bifurcation located in the southern branch of the delta apex (denoted FBN and FBS). At each location, the section-averaged values of SSC are determined from data capturing the spatial distribution of suspended sediment, flow velocity and flow depth, all measured at the same time. More detailed information about the measurement and calibration procedures as well as spatial data of SSC in the observed channel sections can be found in Sassi et al. (2012, 2013). Most sediment observations cover a period of 13 hours, i.e. one complete semidiurnal tidal cycle. Only the observations made on 12-26-2008 cover a period of only 7 hours due to technical difficulties. The observed ranges of section-averaged SSC at these locations are summarized in Table 1.

Observations of SSC at Samarinda, DAN, DAS, FBN, and FBS in the period from November 2008 to January 2009 are used for calibration purposes (Section 5.3) while the sediment data measured on the different dates between February 2009 and October 2009 at Samarinda are employed to validate the model (Section 5.4). Different simulations are performed and the computed SSC are compared to the observations at the measurement locations.

5.2. Different type of errors

To assess the quality of the simulated SSC compared to the observations, different criteria, i.e. temporal error E_t and Pearson's correlation coefficient r, are calculated at the measurement stations. The temporal error E_t is applied as a quantitative estimate of the mean error. The temporal error E_t is computed as:

$$E_t = \frac{\sqrt{\sum_t \left[(C_{ss})_{data} - (C_{ss})_{model} \right]^2}}{\sqrt{\sum_t \left[(C_{ss})_{data} \right]^2}} \tag{17}$$

where $\sum_t$ means the sum over different times, $(C_{ss})_{data}$ and $(C_{ss})_{model}$ are respectively the observations and computed SSC at a specific station. The Pearson's correlation coefficient r is used to analyze the correlation and variable trend of model results in comparison with the field data. The coefficient r is calculated as follows:

$$r = \frac{\sum_t \left(C_{ss} - C_{ss,m} \right)_{data} \left(C_{ss} - C_{ss,m} \right)_{model}}{\sqrt{\sum_t \left(C_{ss} - C_{ss,m} \right)^2_{data}} \sqrt{\sum_t \left(C_{ss} - C_{ss,m} \right)^2_{model}}} \tag{18}$$

where $\left(C_{ss,m} \right)_{data}$ and $\left(C_{ss,m} \right)_{model}$ are the mean value of observed and computed SSC, respectively, at a specific location.

5.3. Calibration results

As mentioned previously, there are three parameters to calibrate, i.e. k_1, β, and M. Different constant values of these parameters are tested, in order to obtain the best fit with the observations of SSC at five stations. The value of each parameter is varied separately,

whilst keeping the other once constant. Among different testing values, several constant values for the three parameters (i.e. k_1=0.04, 0.08, 0.12; β=1.0, 1.25, 1.30; and M=0.00005, 0.00012, 0.00021, 0.00025 kg/m^{2}s) are summarized here. Thirty-six simulations associated with combination of these constant parameters values are performed, with the aim to select the best combination of values for the parameters k_1, β, and M in their typical range of variation. Table 2 presents the parameter values for each simulation as well as the temporal error obtained at each station for the calibration period.

The temporal error of SSC versus the variable values of M and k_1 (and the constant value β=1.25) is shown in Figure 4 while its value versus the variable values of M and β (and the constant value k_1=0.08) is illustrated in Figure 5. It can be observed that the temporal errors at all five stations vary significantly if variable values of parameters are employed. This suggests that the calculated results of SSC are very sensitive to changes in both the erosion rate and the deposition rate, resulting from alternating the value of M and settling velocity (related to k_1 and β), respectively. The optimal parameter set is found to be k_1=0.08, β=1.25, and M=12x10^{-5} kg/m^{2}s. This corresponds to simulation a.18, for which comparisons between calculated and observed SSC during the simulation period are shown in Figure 6 and Figure 7.

Figure 6 shows the comparison between simulation results and data of SSC at Samarinda station. The model reproduces very well the temporal variation of SSC measured on different dates. The temporal error at this station is only about 0.06. In addition, the model seems to be able to represent the variations of SSC associated with neap-spring tidal cycles, besides the semidiurnal tides. During spring tides, SSC variations are significantly higher due to the strong tidal currents. The correlation coefficient between computed and observed SSC is 0.97, revealing that the model very well reproduces the field data on sediment.

Figure 7 depicts the modeled SSC and observations at the four other stations (i.e. DAN, DAS, FBN, and FBS). Again, a very good agreement between computed and observed section-averaged SSC is obtained for the two considered measurement dates. The maximum temporal error at these channel sections is only about 0.20. The coefficient *r* is very close to unity (> 0.96) at all these four stations.

Figure 8 shows the interquartile range of SSC at five stations, which is a measure of statistical dispersion, equal to the difference between the first and third quartiles, of all simulations in Table 2. The simulation corresponding to the best parameter combination set (simulation a.18) is within the interquartile range at all five considered stations. The interquartile range represents the uncertainty in simulations due to the variability of the investigated parameters, and is considered here to represent the uncertainty associated with the best parameter set. Uncertainty typically increases for high SSC values and observations mostly fall within these bounds.

In general, a very good agreement is achieved between the simulation results and observed data at all five stations. The values of the parameters corresponding to simulation a.18 are considered as the optimal ones in the calibration stage.

5.4. Validation results

To validate the model, a simulation for a longer period, six months from February to August 2009, is performed and the results are compared with the observations at Samarinda (Figure 9). An excellent agreement is achieved between the simulated and observed SSC for the three sets of observations corresponding with the validation period. The temporal error is 0.21, which is only slightly greater than the error in the calibration step (simulation a.18). The correlation coefficient *r* between observed and computed SSC is 0.92, which is slightly smaller than the value in simulation a.18, but still indicating a strong positive correlation. A positive value of the covariance between computed and

observed SSC is also arrived at, revealing that the model correctly reproduces the variation trend observed in situ.

As shown in Figure 9, the tide is the key factor controlling SSC variation at both short and medium time-scales at Samarinda station. Both field observations and simulation results show temporal variations of SSC to be controlled by the semidiurnal tide and its associated spring-neap cycle. A decrease of SSC corresponding to the low-flow period between July and August 2009 is observed, during which the river flow varies between 1200 and 2300 m^3/s.

During the low-flow period (Figure 9d), simulations overestimate the observations during ebb and underestimate the observations during flood. These discrepancies may be related to several factors. First, the water discharge imposed at the tributaries was estimated using a rainfall-runoff model that may be plagued with significant uncertainties during the low-flow period, as concluded by Pham Van et al. (2012a). The simulation results of SSC corresponding to the low-flow suggest that the river discharge used in the simulation seems to be overestimated. Second, the contribution of the tidal motion from multiple channels in the delta into the Mahakam River can differ with the seasons. Finally, using a constant roughness coefficient in the simulations may not be entirely appropriate during low-flow conditions.

6. Discussion

Figure 10 illustrates the time-series of daily averaged SSC at Samarinda station during the years 2008-2009. The temporal variation of SSC is obtained by using the optimal values of parameters calibrated and validated in the previous section (i.e. setup of simulation a.18). For comparison, results obtained from a rating curve of the form $C_{ss} = pQ^q$ (Asselman, 1999) are also shown. Note that Q is the water discharge (m^3/s), and p and q are empirically derived regression coefficients. Based on the best linear-fit for the five observations at Samarinda, the values p=0.0136 and q=0.23 are obtained and these values

608 are applied in the calculations. The figure (i.e. Figure 10) shows the increased level of
609 detail that can be obtained with the simulations compared to a simple rating curve
610 approach. During high-flow, both the model and the rating curve simulate the effect of the
611 seasonal variation of river flow reasonably well. However, during the low-flow period,
612 daily averaged SSC variation influenced by the tide, can only be captured by the model.

613 Temporal variations of SSC associated with the variable river discharge appear to be
614 well-represented by the model. For instance, the temporal variation of SSC at Samarinda
615 (see Figure 10) showed that the SSC remains higher during the high flow period from
616 November to April 2009, corresponding to the rainfall period. Moreover, multiple peaks of
617 SSC occurred during the periods December-January and April-May corresponding to the
618 two rainfall peaks in the river catchment (Hidayat et al., 2012).

619 Figure 11 shows an example of the spatial distribution of the computed SSC in the
620 Mahakam River and in the whole delta, obtained from the model at the ebb tidal phase of
621 neap tide, i.e. at 13:50:00 on 03-10-2009. The figure illustrates the significant variation of
622 SSC along the river and in the delta. In the upstream area of the Mahakam River, where the
623 influences of the tide on flow dynamics is smaller than in the delta, and the river flow is a
624 dominant factor controlling sediment transport, high values of SSC are obtained. Close to
625 the delta, where the tidal effects are strong and the flow dynamics is more complicated,
626 SSC changes significantly in space. The figure shows a gradual decrease of SSC from the
627 mouth of the Mahakam River to the delta shore.

628 The simulation results show that SSC in the Mahakam Delta varies in a range between
629 0.001 and 0.16 (kg/m^3). This range is similar to the in situ values obtained by Budhiman et
630 al. (2012) who reported that SSC near the water surface varies from 0.006 to 0.182 (kg/m^3)
631 based on their field measurements performed in May and August 2008 and in August 2009,
632 at 119 field sampling sites distributed in the whole delta. In addition, the computed range
633 of SSC is also in good agreement with the two-week field campaign in September 2003

reported by Storms et al. (2005) who show that SSC in water samples at various sites in the southern river branch and adjacent river mouth of the Mahakam River varies between 0.005 and 0.15 (kg/m^3).

The settling velocity is an important parameter in estimating the net sediment exchange from a river bed or sea bed (Van Leussen, 1999; Wu, 2007). According to Burban et al. (1990), the settling velocity of fine-grained sediment in fresh and sea water environments is often affected by varying factors related to flow shear stress, sediment concentration, salinity, organic matter, *pH*, temperature, and organisms. Observations of such abovementioned physical, chemical, and biological quantities are often limited (Mercier and Delhez, 2007; Winterwerp, 2013; Elskens et al., 2014), especially in coastal regions like the Mahakam Delta. In this deltaic region, the settling velocity of sediment is known to be a strong function of sediment concentration, which is highly variable in a holistic model such that presented here. The best model results were obtained if the settling velocity was simply parameterized by using a power function of the sediment concentration (i.e. $w_s = 0.08C_{ss}^{1.25}$). The computed settling velocity in the delta varies over a wide range between 0.001 and 8.5 mm/s, which is in the typical range of settling velocity for fine-grained sediments in estuarine and deltaic regions (Burban et al., 1990; Lou and Ridd, 1997; Van Leussen, 1999). The effects of salinity, organic matter, *pH*, temperature, and organisms on the settling velocity of fine-grained sediments would be probably considered in the next stages of the research, when field measurements of these physical, chemical, and biological quantities are performed.

The SSC calculations presented here are carried out by using one sediment layer or class only, in which only fine-grained sediment is considered. To realistically simulate the effects of particle size variations in the water column, different sediment classes could be included in a future modelling effort. Fine-grained sediment particles may stick together and form flocs when they collide (Winterwerp, 1998), because of turbulence and the action

of electrostatic forces, as well as the polymers resulting from biological processes that are adsorbed onto the surfaces of the fine-grained sediment particles (Wu, 2007; Van Leussen, 1999). The associated processes may result in variability in sizes and settling velocities of the flocs in space and time. Investigating the influence of flocculation processes is also foreseen in the future to better understand the suspended matter dynamics in the delta as well as in the Makassar Strait, as suggested by Eisma et al (1989). Sassi et al. (2012) suggested that flocculation processes are also important in the tidal river, upstream of the delta.

7. Summary and conclusions

A coupled 2D/1D model including shallow-water and advection-diffusion equations in the framework of the finite element model SLIM has been successfully applied to reproduce suspended sediment transport in the Mahakam land-sea continuum. The aims of the study were to simulate fine-grained sediment transport within the domain of interest of the system, to accurately reproduce the measured SSC at different locations in the delta, and to represent spatial and temporal variations of SSC under the combined influences of river flow and tides in such a complex system. Calibration simulations were performed to establish the best performing values of parameters in the suspended sediment transport module. The model was also validated additionally. A very good agreement was achieved between the computed and observed variation of SSC at different measurement stations in the system, both for the calibration and the validation periods.

The simulation results corresponding to the best parameter set showed that the temporal error of SSC was less than 0.20 and the correlation coefficient between computed and observed sediment concentrations was close to unity. These simulation results were also well within the interquartile range of the measurements, at all five measurement stations. This demonstrates that the coupled 2D/1D model of the SLIM reproduced very well the suspended sediment transport across the land-sea continuum.

Simulation results over a year in 2008-2009 showed that the model was able to accurately simulate the temporal variation of SSC in response to the variation of the river flow. Comparisons of model results with field observations reported in previous studies for the Mahakam Delta were all favorable.

Acknowledgements

The present study was carried out in the framework of the project "Taking up the challenges of multi-scale marine modelling" which is funded by the Communauté Francaise de Belgique under contract ARC 10/15-028 (Actions de recherche concertées) with the aim of developing and using SLIM (www.climate.be/slim). Computational resources have been provided by the supercomputing facilities of the Université catholique de Louvain (CISM/UCL) and the Consortium des Equipements de Calcul Intensif en Fédération Wallonie Bruxelles (CECI) funded by the Fond de la Recherche Scientifique de Belgique (F.R.S-FNRS). Eric Deleersnijder and Sandra Soares-Frazão are honorary research associates with this institution. The authors would like to thank Prof. Iwan Suyatna (Mulawarman University, Indonesia) for sharing the measurement salinity data used for the numerical simulations herein.

Appendix A: Estimating the dispersion coefficient using salinity data

To simulate the salinity transport in the computational domain, the coupling between section-averaged and depth-averaged advection-diffusion equations is applied. These equations are written in the following forms:

$$\frac{\partial(AS)}{\partial t}+\frac{\partial(AuS)}{\partial x}=\frac{\partial}{\partial x}\left(A\kappa\frac{\partial S}{\partial x}\right) \tag{19}$$

$$\frac{\partial(HS)}{\partial t}+\nabla\cdot(HuS)=\nabla\cdot(H\kappa\nabla S). \tag{20}$$

where S (-) is the sectional-averaged salinity in the 1D sub-domain or depth-averaged salinity in the 2D sub-domain and, again, κ is the diffusivity coefficient that is

parameterized under the form of eq. (12). It must be emphasized that equations (19) and (20) are also solved in the framework of the finite element model SLIM by using a discontinuous Galerkin finite element method (with linear shape functions) for the spatial operators and a second-order diagonally implicit Runge-Kutta for the temporal operators.

Salinity data were collected in the period between August 2009 and January 2010 at 60 locations in the tidal channels of the delta and in the delta shore (Figure 2). At each location, salinity was measured in situ at the water surface using water checker Horiba. This dataset covers a representative range of salinity conditions, with values ranging between 2.1 and 34.8 PSU and water depths varying from 1.0 to 42 meters (Suyatna et al., 2010).

The measurement data of salinity mentioned above are used to determine the optimal value of coefficient c_k in eq. (12). The simulation period ranges from July 2009 to end of measurement time, i.e. January 2010. The setup of the hydrodynamic module and the optimal value of the Manning coefficient described in Section 3 are employed to reproduce the flow dynamics in the system. The daily water discharge at the upstream Mahakam River varies between 480 (low-flow conditions) and 5400 m^3/s (high flow conditions). A value of 35 PSU is imposed in the deepest parts of the computational domain (Makassar Strait) while freshwater is entering the domain at upstream boundaries of the Mahakam River and tributaries. The regime condition for salinity is also obtained after a spin up period of one neap-spring tidal cycle (about 15 days).

Several simulations using constant values of c_k in a range between 0.008 and 0.06 are performed. The best match between computed and observed salinity is achieved as shown in Figure 12 when a value c_k=0.018 is employed. The RMS error of salinity in this case is 3.4 PSU, about 10% of observed magnitude of salinity. A few points still lie significantly above the perfect matching line (Figure 12). These points correspond to sampling sites near the coast of the northern area of the delta. In view of the rather limited amount of observed

salinity data, c_k=0.018 is considered to be the appropriate approximate value for determining the diffusivity coefficient in studying SSC in the delta.

The diffusivity coefficient κ corresponding to c_k=0.018 varies in a range between 0.21 and 80 (m^2/s) in the delta while its value equals 3.6 (m^2/s) in the river and tributaries. The latter value is obtained by replacing the mesh size of element in the 2D sub-domain by the length of a segment in the 1D sub-domain. These values of the diffusivity coefficient are in the typical range of dispersion coefficient for the estuaries and coastal regions, as mentioned in Fischer et al. (1979).

References

Allen, G. P., Chambers, J. L. C., 1998. Sedimentation in the modern and Miocene Mahakam delta. *Indonesian Petroleum Association*, Jakarta, p. 236.

Allen, G. P., Laurier, D., Thouvenin, J., 1979. Etude sedimentologique du delta de la Mahakam. *TOTAL Compagnie Française des Petroles, Notes et Mémoires*, Paris, N° 15, 154p.

Ariathuri, R., Krone, R.B., 1976. Finite element model for cohesive sediment transport. Journal of Hydraulic Engineering, 102(3), 323-338.

Asselman, N. E. M., 1999. Suspended sediment dynamics in a large drainage basin: the River Rhine. Hydrological processes, 13, 1437-1450.

Bernard, P. E., Chevaugeon, N., Legat, V., Deleersnijder, E., Remacle, J.-F. 2007. High-order h-adaptive discontinuous Galerkin methods for ocean modeling. Ocean Dynamics, 57, 109-121 (+Erratum, 2007, 57, 579-580).

Budhiman, S., Salama, S. M., Vekerdy, Z., Verhoef W., 2012. Deriving optical properties of Mahakam Delta coastal waters, Indonesia using *in situ* measurements and ocean color model inversion. ISPRS Journal of Photogrammetry and Remote Sensing, 68, 157-169.

Burban, P.-Y., Xu, Y.-J., McNeil, J., Lick W., 1990. Settling speeds of floes in fresh water and seawater. Journal of Geophysical Research, 95(C10), 18213-18220.

Budiyanto, F., Lestari, 2013. Study of metal contaminant level in the Mahakam Delta: Sediments and dissolved metal perspectives. Journal of Coastal Development, 16 (2),

147-157.

Buschman, F.A., Hoitink, A.J.F., De Jong, S.M., Hoekstra, P., Hidayat, H., Sassi, M. G., 2012. Suspended sediment load in the tidal zone of an Indonesian river. Hydrology and Earth System Sciences, 16 (11), 4191-4204.

Chaîneau, C.-H., Miné, J., Suripno, 2010. The integration of biodiversity conservation with oil and gas exploration in sensitive tropical environments. Biodiversity and Conservation, 19(2), 587-600.

Comblen, R., Lambrechts, J., Remacle, J.-F., Legat V., 2010. Practical evaluation of five partly discontinuous finite element pairs for the non-conservative shallow water equations. International Journal for Numerical Methods in Fluids, 63, 701-724.

de Brye, B., de Brauwere, A., Gourgue, O., Kärnä, T., Lambrechts, J., Comblen, R., Deleersnijder E., 2010. A finite-element, multi-scale model of the Scheldt tributaries, river, estuary and ROFI. Coastal Engineering, 57, 850-863.

de Brye, B., Schellen, S., Sassi, M., Vermeulen, B., Deleersnijder, E., Hoitink, A.J.F., 2011. Preliminary results of a finite-element, multi-scale model of the Mahakam Delta (Indonesia). Ocean Dynamics, 61, 1107-1120.

Darby, S. E., Thorne, C. R., 1996. Predicting stage-discharge curves in channels with bank vegetation. Journal of Hydraulic Engineering, 122(10), 583-586.

Deleersnijder, E., Lermusiaux P., (Editors) 2008. Multi-scale modeling: Nested-grid and unstructured-mesh approaches. Ocean Dynamics (Special issue), 58, 335–498.

Dutrieux, E., 1991. Study of the ecological functioning of the Mahakam delta (east Kalimantan, Indonesia). Estuarine, Coastal and Shelf Science, 32(4), 415-420.

Edmonds, D. A., Slingerland, R. L., 2010. Significant effect of sediment cohesive on delta morphology. Nature Geoscience, 3, 105 – 109.

Eisma, D., Kalf, J., Karmini, M., Marok, W.G., Van Put, A., Bernard, P., Van Grieken, R., 1989. Dispersal of suspended matter in Makassar Strait and the Flores Basin. Netherlands Journal of Sea Research, 24(4), 383-398.

Egbert, G.D., Bennet, A.F., Foreman, M.G.G., 1994. TOPEX/POSEIDON tides estimated using a global inverse model. Journal of Geophysical Research, 99(C12), 24821-24852.

Elskens, M., Gourgue, O., Baeyens, W., Chou, L., Deleersnijder, E., Leermakers, M., de Brauwere, A., 2014. Modelling metal speciation in the Scheldt Estuary: Combining a

flexible-resolution transport model with empirical functions. Science of The Total Environment, 476-477, 346-358.

Einstein, H.A., Krone, R.B., 1962. Experiments to determine modes of cohesive sediment transport in salt water. Journal of Geophysical Research, 67, 1451-1461.

Fischer, H. B, List, E.J., Koh, R.C.Y., Imberger, J., Brooks, N.H., 1979. Mixing in inland and coastal waters. Academic Press, New York.

Gastaldo, R.A., Huc, A.-Y., 1992. Sediment Facies, Depositional Environments, and distribution of Phytoclasts in the Recent Mahakam River Delta, Kalimantan, Indonesia. Palaios, 7 (6), 574-590.

Gastaldo, R.A., Allen, G. P., Huc, A.-Y., 1995. The tidal character of fluvial sediments of the modern Mahakam River delta, Kalimantan, Indonesia. Spec. Publs int. Ass. Sediment, 24, 171-181.

Geuzaine, C., Remacle, J.-F., 2009. GMSH: a finite element mesh generator with built-in pre-and post-processing facilities. International Journal for Numerical Method in Engineering, 79(11), 1309-1331.

Gourgue, O., Baeyens, W., Chen, M. S., de Brauwere, A., de Brye, B., Deleersnijder, E., Elskens, M., Legat V., 2013. A depth-averaged two-dimensional sediment transport model for environmental studies in the Scheldt Estuary and tidal river network. Journal of Marine Systems, 128, 27-39.

Gong, W., Shen, J., 2010. A model diagnostic study of age of river-borne sediment transport in the tidal York River Estuar. Environmental Fluid Mechanics, 10, 177-196.

Hardy, M. J., Wrenn, J. H., 2009. Palynomorph distribution in modern tropical deltaic and shelf sediments–Mahakam Delta, Borneo, Indonesia. Palynology, 33(2), 19-42.

Hadi, S., Ningsih, N.S., Tarya, A., 2006. Study on seasonal variation of cohesive suspended sediment transport in estuary of Mahakam Delta by using numerical model. Jurnal Teknik Sipil, 13(1), 11-22.

Hidayat, H., Vermeulen, B., Sassi, M., Torfs, P.J.J.F., Hoitink, A.J.F., 2011. Discharge estimation in a backwater affected meandering river. Hydrology and Earth System Sciences Discussions, 8, 2667-2697.

Hidayat, H., Hoekman, D.H., Vissers, M.A.M., Hoitink, A.J.F., 2012. Flood occurrence mapping of the middle Mahakam lowland area using satellite radar. Hydrology and Earth System Sciences, 16(7), 1805-1816.

Hoitink, A.J.F., 2004. Tidally-induced clouds of suspended sediment connected to shallow-water coral reefs. Marine Geology, 208(1), 13-31.

Kärnä, T., de Brye, B., Gourgue, O., Lambrechts, J., Comblen, R., Legat, V., Deleersnijder, E., 2011. A fully implicit wetting–drying method for DG-FEM shallow water models, with an application to the Scheldt Estuary. Computer Methods in Applied Mechanics and Engineering, 200, 509-524.

Kirk Ziegler, C., Nisbet, B.S., 1994. Fine-grained sediment transport in Pawtuxet River, Rhode Island. Journal of Hydraulic Engineering, 120(5), 561-576.

Kirk Ziegler, C., Nisbet, B.S., 1995. Long-term simulation of fine-grained sediment transport in large reservoir. Journal of Hydraulic Engineering, 121(11), 773-781.

Lambrechts, J., Comblen, R., Legat, V., Geuzaine, C., Remacle, J.-F., 2008a. Multiscale mesh generation on the phere. Ocean Dynamic, 58, 461-473.

Lambrechts, J., Hanert, E., Deleersnijder, E., Bernard, P.-E., Legat, V., Remacle, J.-F., Wolanski, E., 2008b. A multi-scale model of the hydrodynamics of the whole Great Barrier Reef. Estuarine, Coastal and Shelf Science, 79, 143-151.

Lambrechts, J., Humphrey, C., McKinna, L., Gourgue, O., Fabricius, K.E., Mehta, A.J., Lewis, S., Wolanski, E., 2010. Importance of wave-induced bed liquefaction in the fine sediment budget of Cleveland Bay, Great Barrier Reef. Estuarine, Coastal and Shelf Science, 89, 154-162.

Lang, G., Shubert, R., Markofsky, M., Fanger, H.U., Grabemann, I., Neumann, H.L., Riethmuller, R., 1989. Data interpretation and numerical modeling of the mud and suspended sediment experiment 1985. Journal of Geophysical Research, 94(C10), 14318-14393.

Le Hir, P., Monbet, Y., Orvain, F., 2007. Sediment erodability in sediment transport modelling: Can we account for biota effects?. Continental Shelf Research, 27, 1116-1142.

Lou, J., Ridd, P.V., 1997. Modelling of suspended sediment transport in coastal area under waves and currents. Estuarine, Coastal and Shelf Science, 45, 1-16.

Lukman, Yoga, G.P., Widiyanto, T., Ridwansyad, I., Nomosatrio, S., 2006. Physical characteristics and mangrove community in the north part of Mahakam Delta in East Kalimanta-Indonesia. Limnotek, 13(1), 1-8.

Mandang, I., Yanagi, T., 2009. Cohesive sediment transport in the 3D-hydrodynamic-baroclinic circulation model in the Mahakam Estuary, East Kalimantan, Indonesia. Coastal Marine Science, 32(3), 1-13.

Martini, P., Carniello, L., Avanzi, C., 2004. Two dimensional modelling of flood flows and suspended sediment transport: the case of Brenta river, Veneto (Italy). Natural Hazards and Earth System Sciences, 4, 165-181.

Mehta, A.J., Partheniades, E., 1975. An investigation of the depositional properties of flocculated fine sediments. Journal of Hydraulic Research, 12(4), 361-381.

Mercier, C., Delhez, E.J.M., 2007. Diagnosis of the sediment transport in the Belgian Coastal Zone. Estuarine, Coastal and Shelf Science, 74, 670-683.

Neumeier, U., Lucas, C. H., Collins, M., 2006. Erodibility and erosion patterns of mudflat sediments investigated using annular flume. Aquatic Ecology, 40(4), 543-554.

Okubo, A., 1971. Oceanic diffusion diagram. Deep-Sea Research, 18,789-802.

Partheniades, E., 1965. Erosion and deposition of cohesive soils. Journal of the Hydraulic Division, 91, 105-139.

Pham Van, C., de Brye, B., Soares-Frazão, S., Deleersnijder, E., Hoitink, A.J.F., Sassi, M., Hidayat, H., 2012a. Modelling of salinity distribution and water age in the Mahakam Delta, Indonesia. *International Conference on Estuaries and Coasts: ICEC2012*, Hanoi, Vietnam, 120-127.

Pham Van, C., de Brye, B., Soares-Frazão, S., Deleersnijder, E., 2012b. Preliminary results of a numerical model of suspended sediment in the Mahakam Delta. *Coastlab12*, Ghent, Belgium, 259-260.

Pham Van, C., de Brye B., Deleersnijder, E., Hoitink, A.J.F., Sassi, M.G., Spinewine, B., Hidayat, H., Soares-Frazão, S. Simulations of flow in the tropical river-lake-delta system of the Mahakam land-sea continuum, Indonesia. Journal of Hydrodynamics, under review.

Roberts, H.H., Sydow, J., 2003. Later quaternary stratigraphy and sedimentology of the offshore Mahakam delta, East Kalimantan (Indonesia). Tropical Deltas of Southeast Asia: Sedimentology, Stratigraphy, and Petroleum Geology, 76, 125-145.

Sanford, L.P., Maa, J.P.Y., 2001. A unified erosion formulation for fine sediments. Marine Geology, 179, 9-23.

Sassi, M., Hoitink, A.J.F., de Brye, B., Vermeulen, B., Deleersnijder, E., 2011. Tidal impact on the division of river discharge over distributary channels in the Mahakam Delta. Ocean Dynamics, 61, 2211-2228.

Sassi, M., Hoitink, A.J.F., Vermeulen, B., 2012. Impact of sound attenuation by suspended sediment on ADCP backscatter calibrations. Water Resources Research, 48, *W09520, doi:*10.1029/2012WR012008.

Sassi, M., Hoitink, A.J.F., Vermeulen, B., Hidayat, H., 2013. Sediment discharge division at two tidally influenced river bifurcations. Water Resources Research, 49(4),2119-2134, doi:10.1002/wrcr.20216.

Smagorinsky, J., 1963. General circulation experiments with the primitive equations. Monthly Weather Review, 91, 99-164.

Storms, J.E.A., Hoogendoorn, R.M., Dam, R.A.C., Hoitink, A.J.F., Koonenberg, S.B., 2005. Late-Holocene evolution of the Mahakam delta, East Kalimantan, Indonesia. Sedimentary Geology, 180, 149-166.

Susanto, R.D., Ffield, A., Gordon, A., Adi, T.R., 2012. Variability of Indonesian throughflow within Makassar Strait, 2004-2009. *Journal of Geophysical Research*, 117, C09013, doi:10.1029/2012JC008096.

Suyatna, I., Bratawinata, A.A., Sidik, A.S., Ruchaemi A.A. 2010. Demersal fishes and their distribution in estuarine waters of Mahakam Delta, East Kalimantan. Biodiversitas, 10(4), 204-210.

Turner, A., Millward, G.E., 2002. Suspended particles: Their role in estuarine biogeochemical cycle. Estuarine, Coastal and Shelf Science, 55, 857-883.

van Zwieten, P.A.M, Sidik, A.S., Noryadi, Suyatna, I., Abdunnur, 2006. Aquatic food production in the coastal zone: data-based perceptions on the trade-off between mariculture and fisheries production of the Mahakam delta and estuary, East Kalimantan. *Environment and livelihoods in tropical coastal zones*, vol. 219, edited by C. T. Hoanh et al., pp. 219-236, CABI publishing, UK.

Van Leussen, W., 1999. The variability of settling velocities of suspended fine-grained sediment in the Ems Estuary. Journal of Sea Research, 41, 109-118.

Zhang, S.Q., 1999. One-D and two-D combined model for estuary sedimentation.

International Journal of Sediment Research, 14(1), 37-45.

White, L., Legat, V., Deleersnijder, E., 2008. Tracer conservation for three-dimensional, finite-element, free-surface, ocean modeling on moving prismatic meshes. Monthly Weather Review, 136, 420–442.

Winterwerp, J. C., 1998. A simple model for turbulence induced flocculation of cohesive sediment. Journal of Hydraulic Engineering, 36(3), 309-326.

Winterwerp, J.C., 2013. The physical analysis of muddy sedimentation processes. *Treatise on Estuarine and Coastal Science*, 2, 311-360.

Wu, W., 2007. Computational river dynamics, Tayler & Francis, London, UK.

Wu, W., Li, Y., 1992. One- and two-dimensional nesting mathematical model for river flow and sedimentation. *The 5th international Symposium on River Sedimentation*, Karlsruhe, Germany, pp. 547-554.

Wu, Y., Falconer, R., Lin, B., 2005. Modelling trace metal concentration distributions in estuarine waters. Estuarine Coastal and Shelf Science, 64, 699-709.

Tables

Table 1 Suspended sediment concentration data in the Mahakam River and its delta

Stations	Date	Tide	Range of suspended sediment (kg/m^3)	Data being used for
Samarinda	11-30-2008	Spring	0.012-0.154	calibration
	01-17-2009	Neap		
	03-12-2009	Neap		validation
	05-24-2009	Neap		
	08-06-2009	Neap		
DAN and DAS	12-26-2008	Spring	0.005-0.110	calibration
	01-04-2009	Neap		
FBN and FBS	12-27-2008	Spring	0.001-0.100	calibration
	01-03-2009	Neap		

Table 2 Temporal errors (E_t) at measurement stations in the computational domain

Sim.	Parameters			E_t				
	k_1	β	M (x10^{-5})	Samarinda	DAN	DAS	FBN	FBS
a.01	0.04	1.0	5	0.3628	0.2306	0.2608	0.2922	0.3070
a.02			12	0.1095	0.2360	0.2495	0.2385	0.1843
a.03			21	0.3447	0.6172	0.6005	0.6003	0.4851
a.04			25	0.4598	0.7636	0.7393	0.7443	0.6107
a.05		1.25	5	0.1596	0.1227	0.1569	0.1497	0.1781
a.06			12	0.2801	0.5885	0.5776	0.5433	0.5056
a.07			21	0.6268	1.0319	1.0022	0.9863	0.8936
a.08			25	0.7553	1.1960	1.1592	1.1500	1.0385
a.09		1.30	5	0.1216	0.1753	0.1935	0.1645	0.2018
a.10			12	0.3292	0.6638	0.6496	0.6103	0.5785
a.11			21	0.6836	1.1163	1.0840	1.0645	0.9773
a.12			25	0.8140	1.2833	1.2439	1.2313	1.1251
a.13	0.08	1.0	5	0.5490	0.4550	0.4692	0.4805	0.5055
a.14			12	0.2423	0.1746	0.2140	0.2167	0.2560
a.15			21	0.0916	0.1842	0.1956	0.2078	0.1426
a.16			25	0.1322	0.2755	0.2705	0.2874	0.1863
a.17		1.25	5	0.3769	0.2242	0.2554	0.2846	0.3014
a.18			12	***0.0608***	***0.1858***	***0.2002***	***0.2034***	***0.1750***
a.19			21	0.2132	0.5046	0.4845	0.4937	0.4067
a.20			25	0.3014	0.6245	0.5974	0.6094	0.5078
a.21		1.30	5	0.3410	0.1780	0.2149	0.2471	0.2638
a.22			12	0.0767	0.2419	0.2491	0.2476	0.2139
a.23			21	0.2582	0.5751	0.5517	0.5586	0.4747
a.24			25	0.3507	0.6986	0.6686	0.6785	0.5797
a.25	0.12	1.0	5	0.6316	0.5537	0.5663	0.5707	0.5962
a.26			12	0.4335	0.3131	0.3409	0.3381	0.3841
a.27			21	0.2602	0.1329	0.1776	0.1780	0.2090
a.28			25	0.2009	0.1216	0.1575	0.1658	0.1606
a.29		1.25	5	0.4795	0.3499	0.3715	0.3899	0.4097
a.30			12	0.2420	0.0946	0.1452	0.1599	0.1793
a.31			21	0.0968	0.2699	0.2641	0.2814	0.2099
a.32			25	0.1223	0.3674	0.3506	0.3697	0.2811
a.33		1.30	5	0.4472	0.3063	0.3307	0.3525	0.3712
a.34			12	0.2038	0.0931	0.1376	0.1536	0.1593
a.35			21	0.1020	0.3308	0.3190	0.3345	0.2609
a.36			25	0.1542	0.4329	0.4116	0.4293	0.3409

Figures

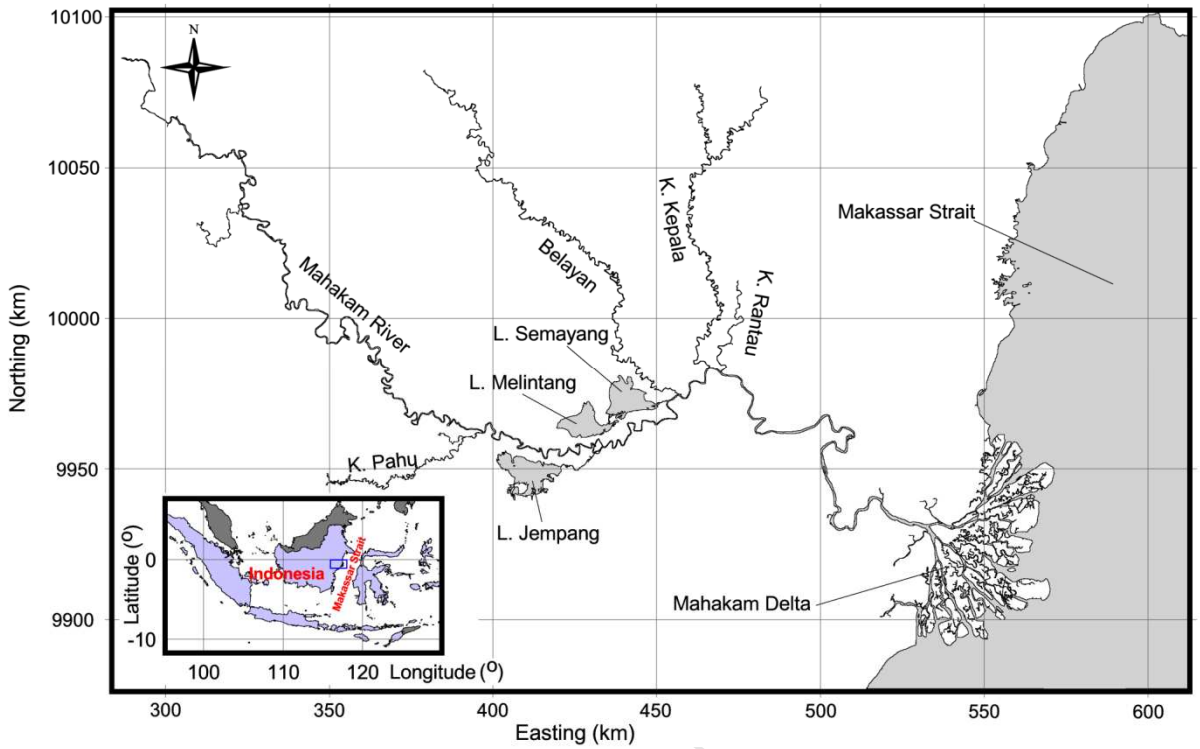

Figure 1. Map of the Mahakam River, main tributaries, and delta

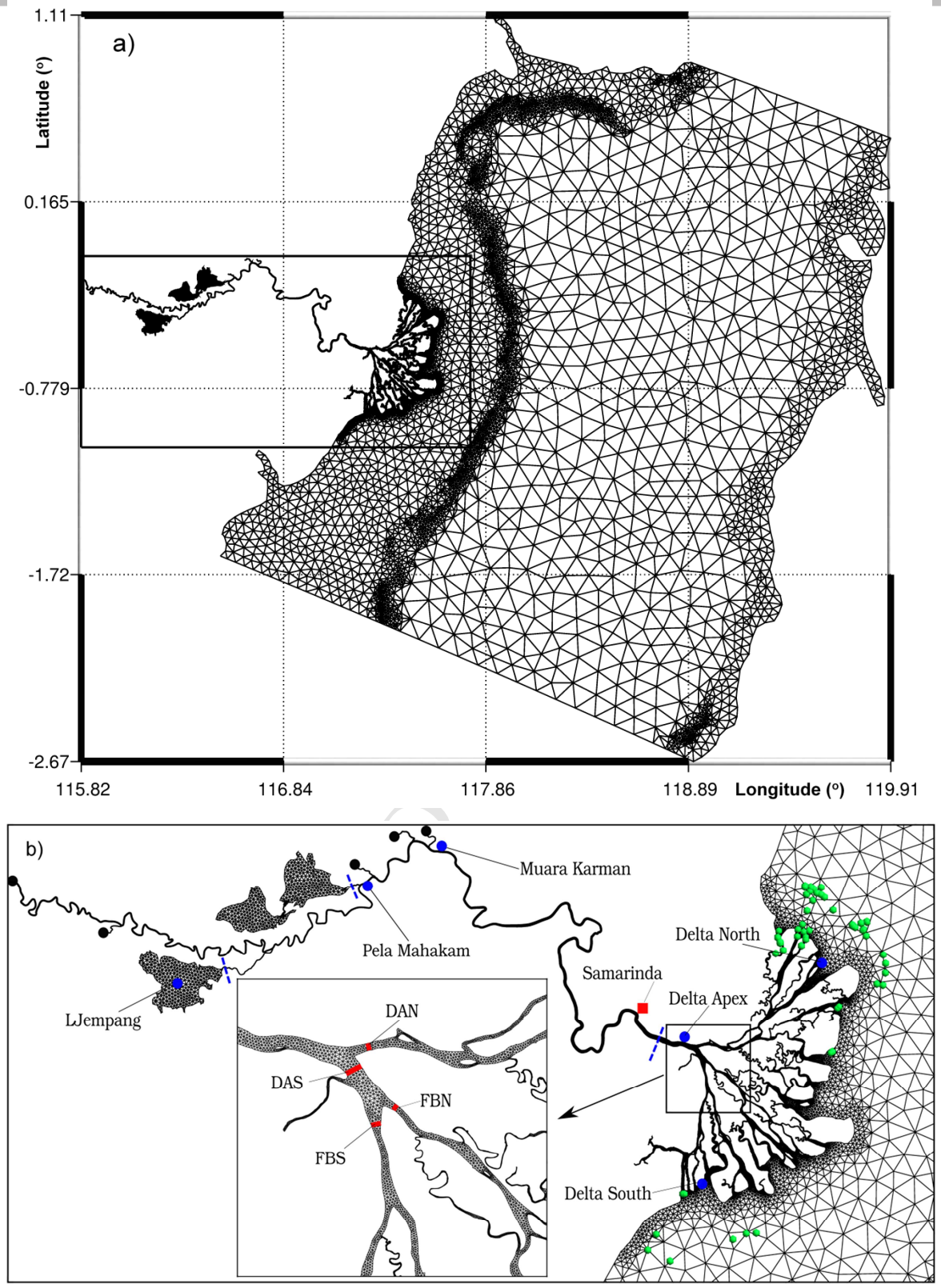

Figure 2. Grid of the model domain: a) complete mesh and b) zoom on upstream domain and delta, also showing the connection between the 1D and 2D models (*dashed-blue lines*), the upstream boundary locations (*back dots*), the sediment and water discharge stations (*red squares*), the water elevation station (*blue dots*), and field sampling sites of salinity (*green dots*)

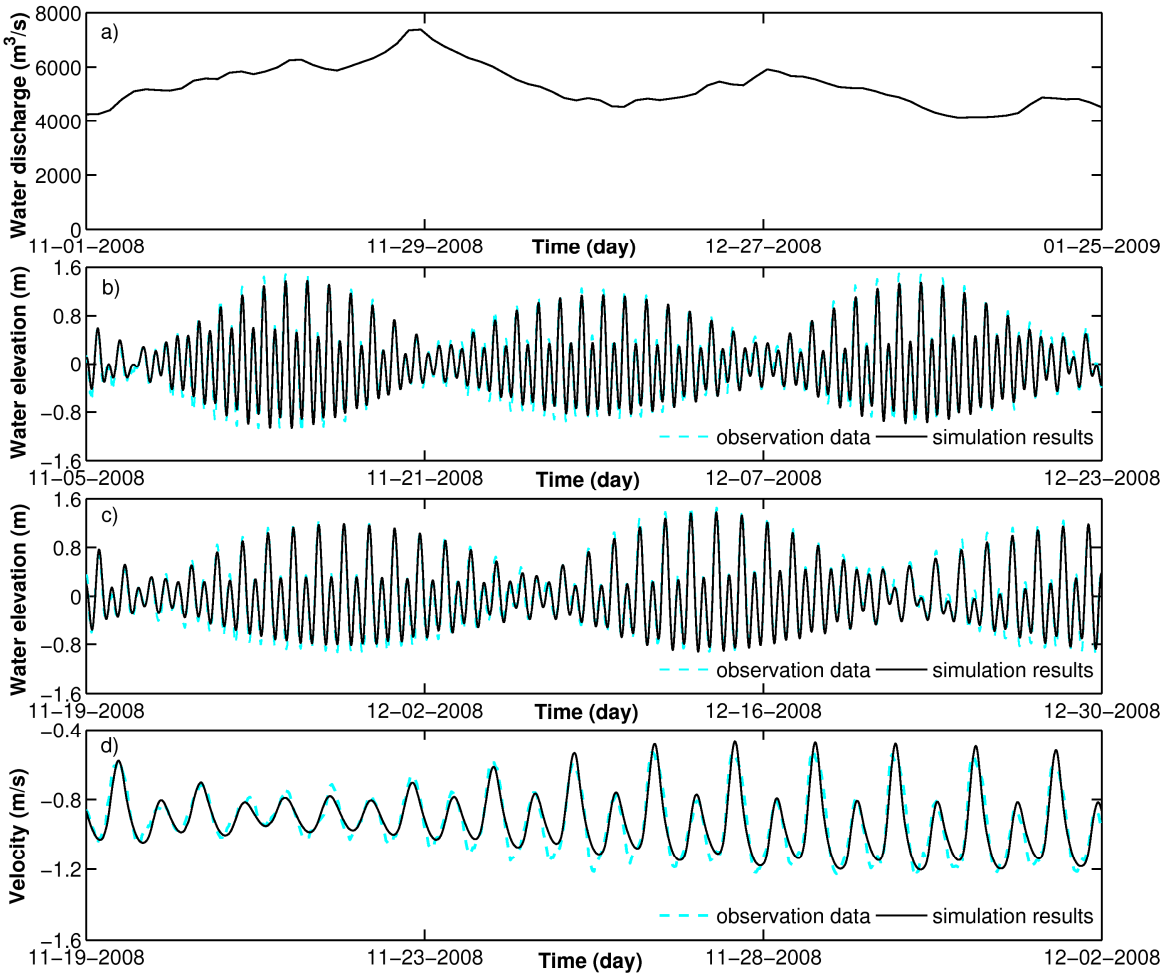

Figure 3. Validation results in the hydrodynamic module: a) water discharge at upstream boundary, b) computed and observed water elevation at Delta North, c) computed and observed water elevation at Delta South, and d) predicted and measured sectional-averaged velocity at Samarinda, where negative velocity coincides with seaward direction

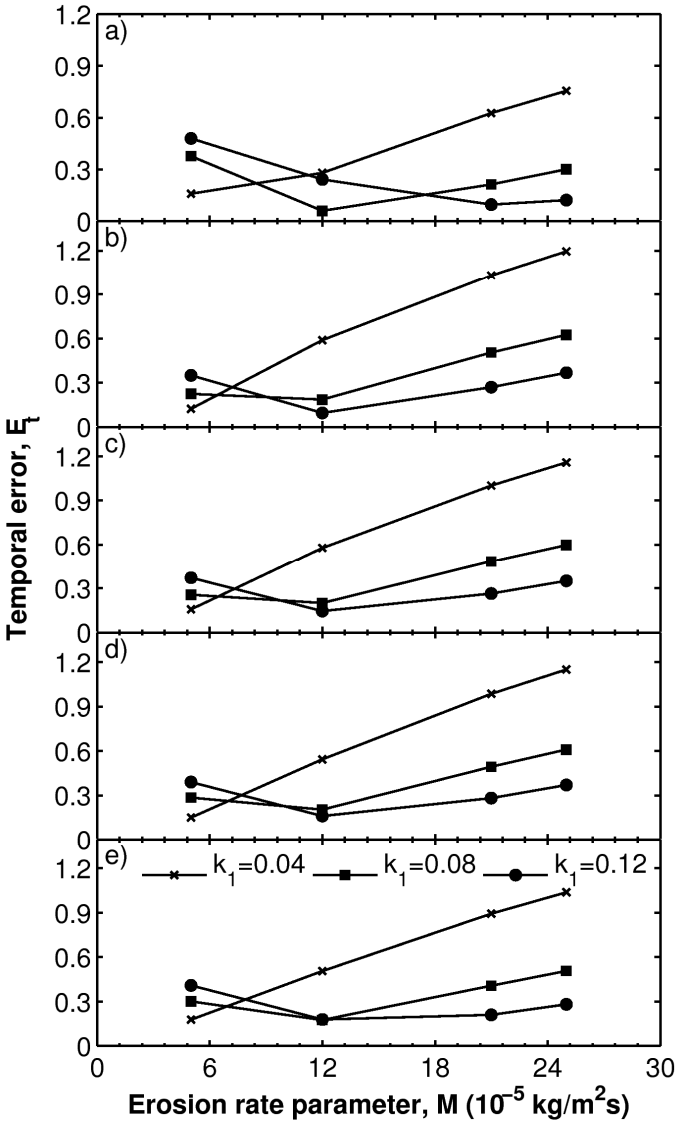

Figure 4. Temporal error of SSC versus the variable values of M and k_1 (and the constant value β=1.25), at: a) Samarinda, b) DAN, c) DAS, d) FBN, and e) FBS stations

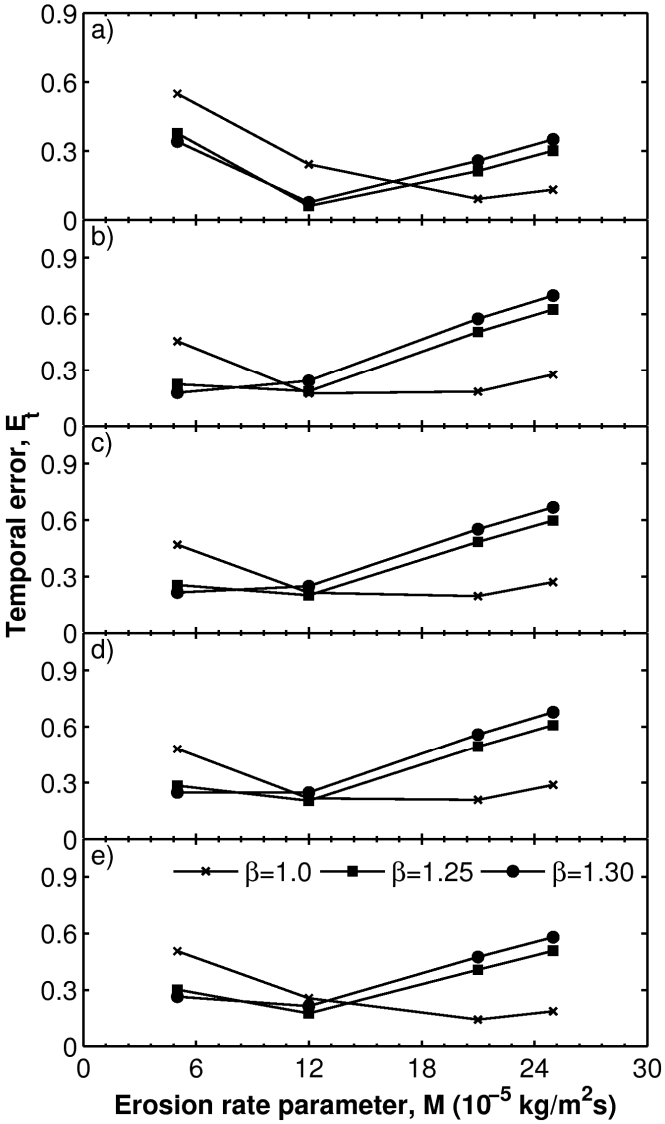

Figure 5. Temporal error of SSC versus the variable values of M and β (and the constant value k_1=0.08), at: a) Samarinda, b) DAN, c) DAS, d) FBN, and e) FBS stations

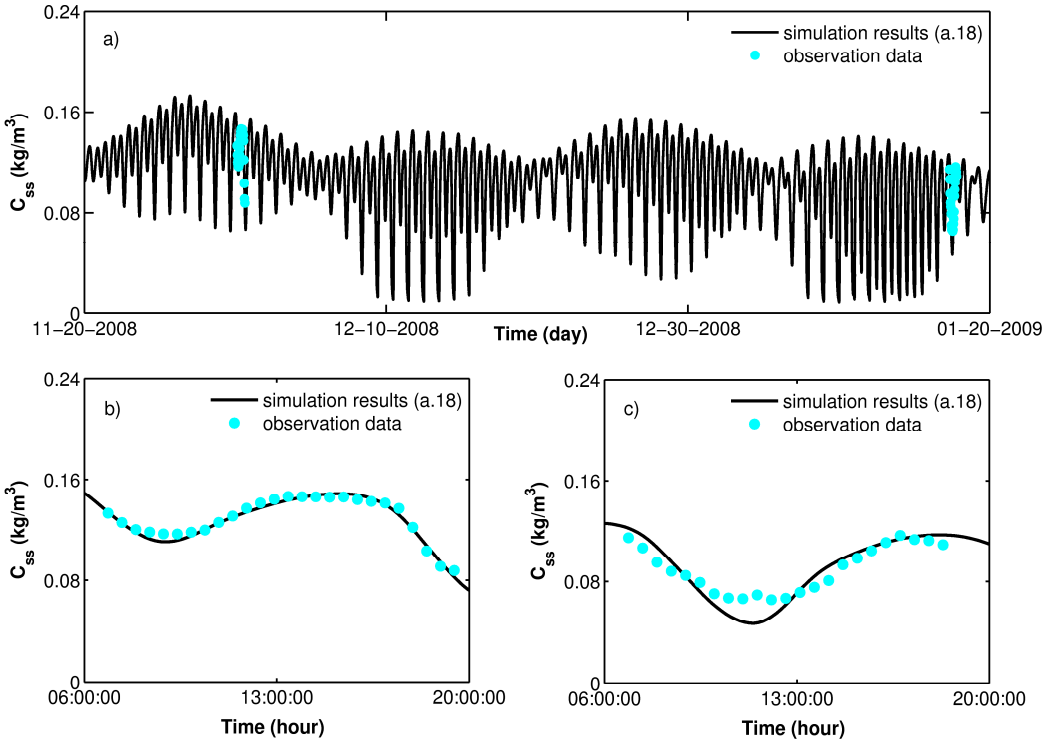

Figure 6. Observed and simulated SSC at Samarinda: a) all simulation period, b) zoom on 11-30-2008, and c) zoom on 01-17-2009 in the calibration step

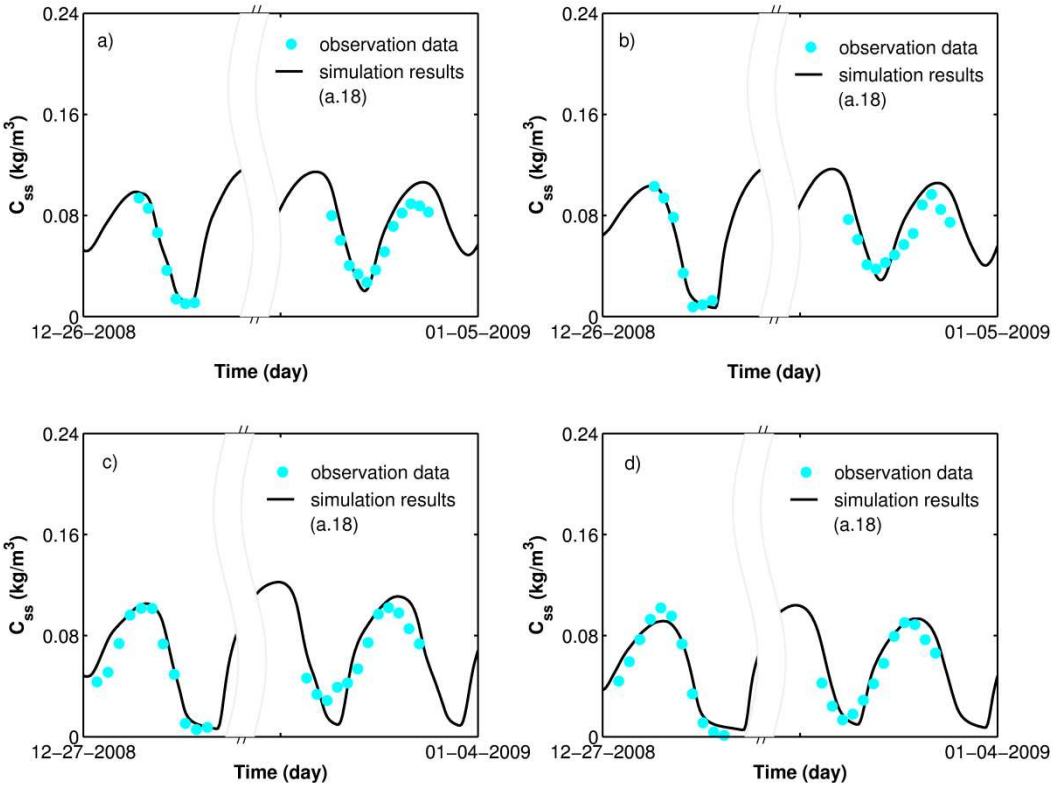

Figure 7. Observed data and simulation results of SSC, at: a) DAN, b) DAS, c) FBN, and d) FBS stations in the calibration step

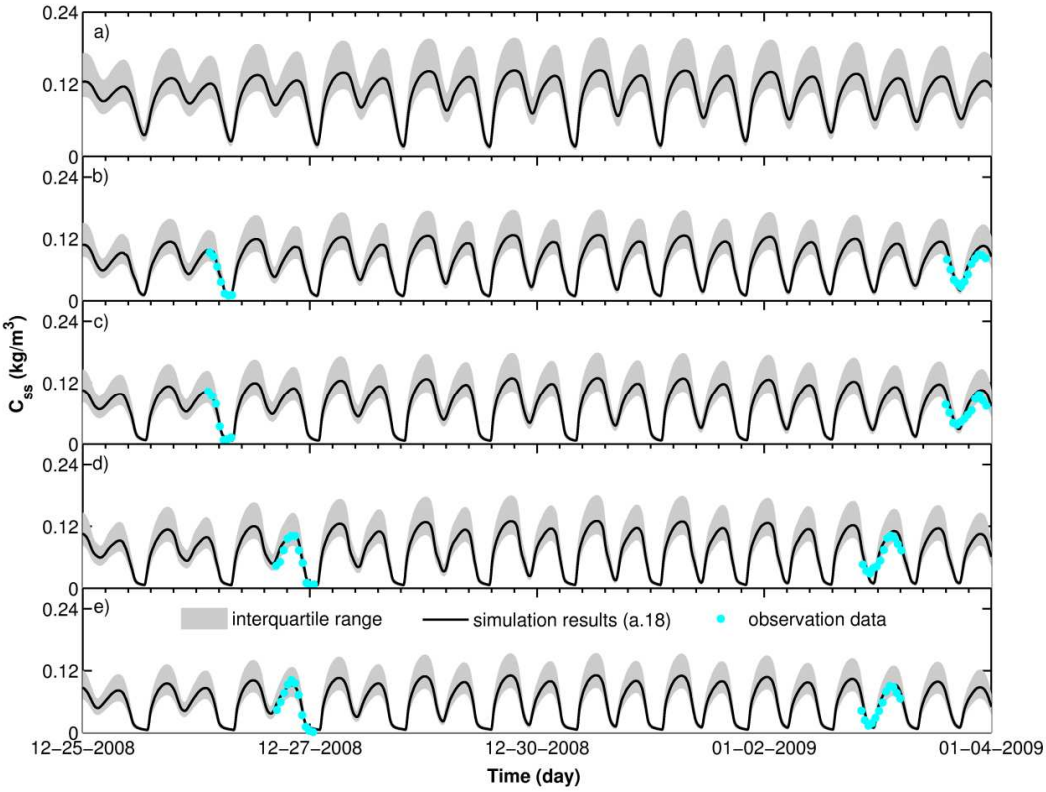

Figure 8. Interquartile range of SSC at: a) Samarinda, b) DAN, c) DAS, d) FBN, and e) FBS stations. At each station, the interquartile range is carried out based on thirty-six simulations in the calibration step

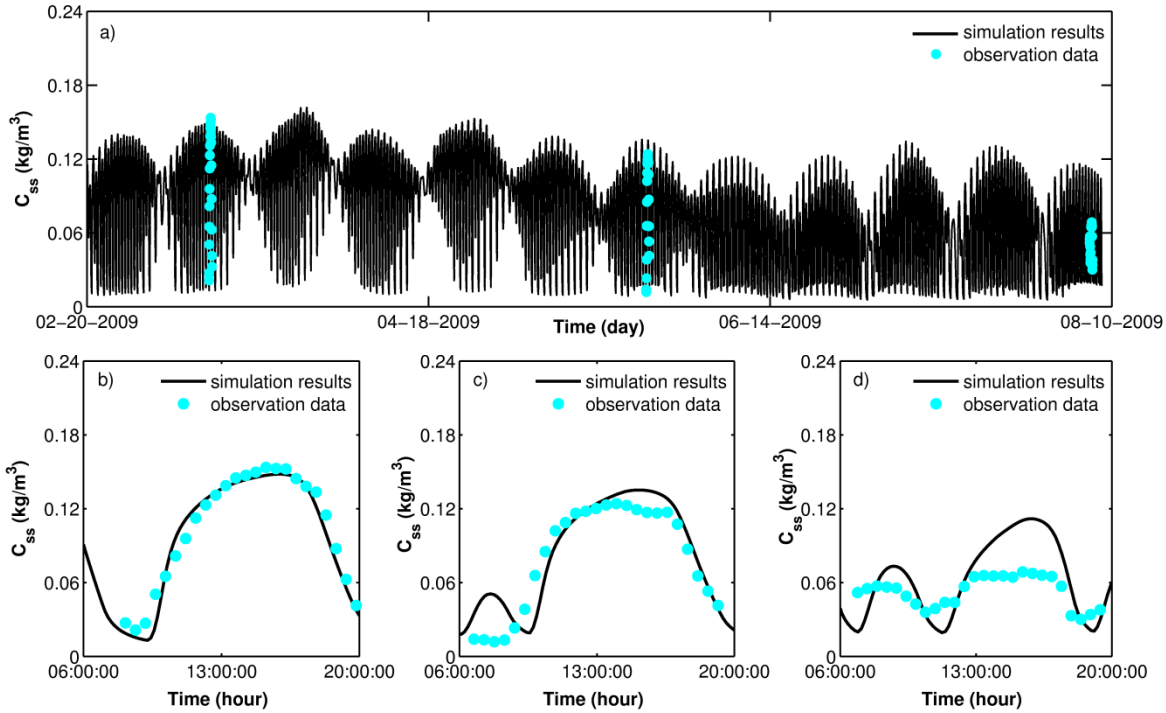

Figure 9. Observed and simulated SSC at Samarinda in the validation step: a) all simulation period of 6 months, b) zoom on 03-12-2009, c) zoom on 05-24-2009, and d) zoom on 08-06-2009. The long-term simulation results are presented for validating the optimal values of parameters (a.18) obtained in the calibration step

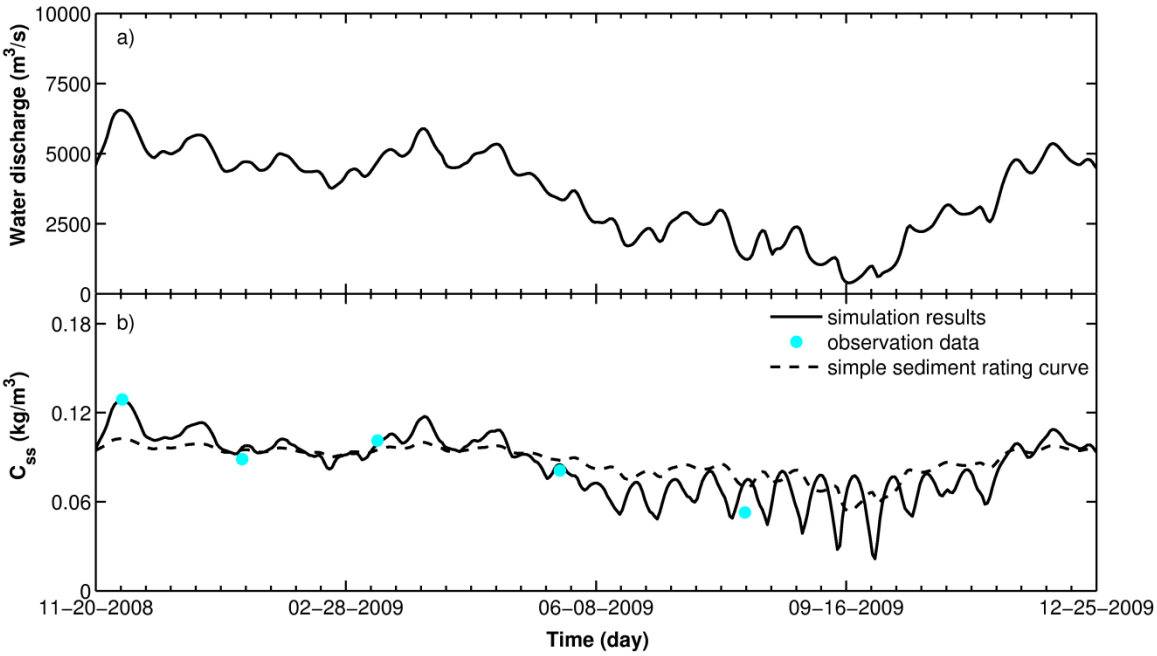

Figure 10. Temporal variation of simulation results in the long period from November 2008 to December 2009: a) daily water discharge and b) daily averaged SSC at Samarinda. The results obtained from a simple sediment curve are presented to show how much detail the model adds compared to its' simple rating curve approach

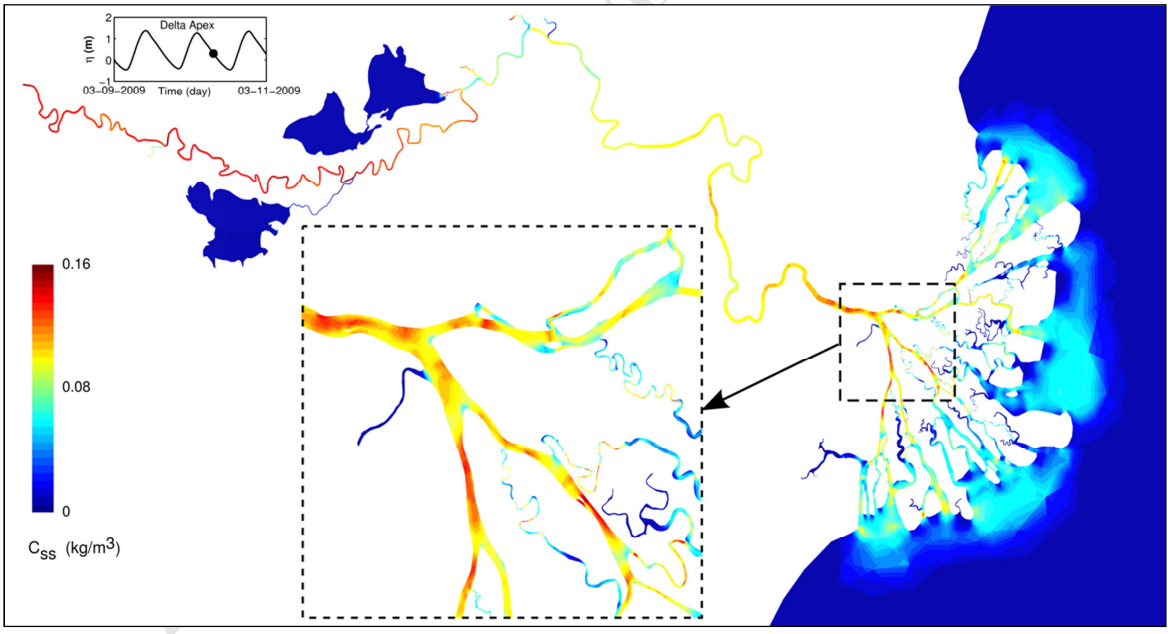

Figure 11. Spatial distribution of SSC in the Mahakam River and in the whole delta, obtained from the model at 13:50:00 on 03-10-2009 that corresponds to the ebb phase of neap tide. Bottom inset is included in order to close view the variation of SSC around the delta apex

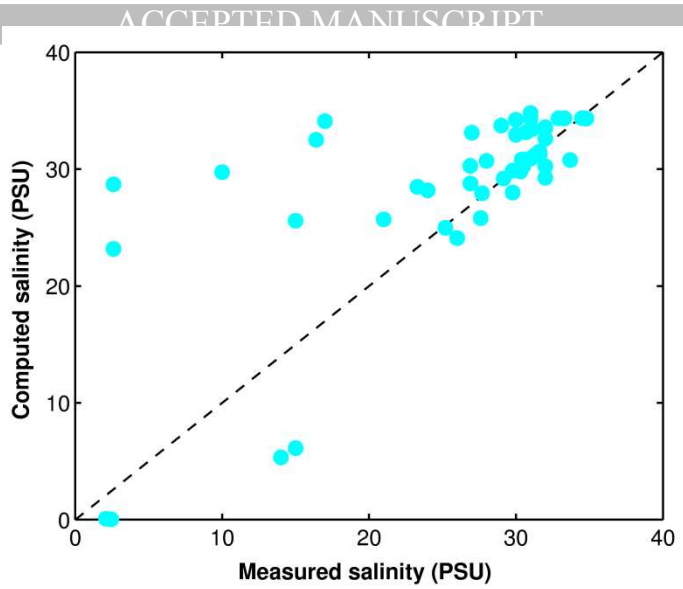

Figure 12. Measured data and computed results of salinity at all field sampling sites. The dash line indicates the perfect fit between computed results and measured data. The computed results are obtained when diffusivity coefficient is parameterized using the Okubo formulation, with the coefficient c_k=0.018

Highlights

- An unstructured-mesh, finite element model allows for the multi-scale simulation of fine-grained sediment dynamics in a land-sea continuum.
- Key model parameters are calibrated using field data.
- The model is able to reproduce very well the measurements made at a number of stations.